HHS Public Access

Author manuscript

Cell Metab. Author manuscript; available in PMC 2021 January 07.

Published in final edited form as:

Cell Metab. 2020 January 07; 31(1): 115–130.e6. doi:10.1016/j.cmet.2019.10.005.

Microbial metabolite signaling is required for systemic iron homeostasis.

Nupur K. Das[1], **Andrew J. Schwartz**[1], **Gabrielle Barthel**[1], **Naohiro Inohara**[2], **Qing Liu**[9], **Amanda Sankar**[3], **David Hill**[8], **Xiaoya Ma**[1], **Olivia Lamberg**[1], **Matthew K. Schnizlein**[6], **Juan L Arqués**[10], **Jason R. Spence**[4,8], **Gabriel Nunez**[2], **Andrew D. Patterson**[9], **Duxin Sun**[7], **Vincent B. Young**[5,6], **Yatrik M. Shah**[1,8,*]

[1]Department of Molecular & Integrative Physiology, University of Michigan, Ann Arbor, MI, 48109, USA.

[2]Department of Pathology and Comprehensive Cancer Center, University of Michigan, Ann Arbor, MI, 48109, USA.

[3]Department of Pediatrics, Division of Hematology-Oncology, University of Michigan, Ann Arbor, MI, 48109, USA.

[4]Department of Cell and Developmental Biology, University of Michigan, Ann Arbor, MI, 48109, USA.

[5]Department of Internal Medicine, Division of Infectious Disease, University of Michigan, Ann Arbor, MI, 48109, USA.

[6]Department of Microbiology and Immunology, University of Michigan, Ann Arbor, MI, 48109, USA.

[7]College of Pharmacy, University of Michigan, Ann Arbor, MI, 48109, USA.

[8]Department of Internal Medicine, Division of Gastroenterology, University of Michigan, Ann Arbor, MI, 48109, USA.

[9]Department of Veterinary and Biomedical Sciences, The Pennsylvania State University, University Park, PA 16802, USA.

[10]Departamento Tecnología de Alimentos, INIA, Carretera de La Coruña Km 7, Madrid 28040, Spain.

[*]Lead Contact: Tel: +1 734 6150567; Fax: +1 734 9368813; shahy@umich.edu.

Author Contributions

N.K.D. and Y.M.S. conceived and designed the study. N.K.D., A.J.S., G.B., N.I., Q.L., J.L.A., J.R.S., G.N. A.D.P, D.S., V.B.Y. developed the methodologies. N.K.D., A.J.S., G.B., N.I., Q.L., A.S., D.H., X.M., O.L., and M.K.S. acquired the data. N.K.D., A.J.S., G.B., N.I., M.K.S and Y.M.S. analyzed and interpreted the data. N.K.D. and Y.M.S. wrote the manuscript. Y.M.S. supervised the study.

Declaration of Interests

The authors declare no competing interests.

Summary

Iron is a central micronutrient needed by all living organisms. Competition for iron in the intestinal tract is essential for the maintenance of indigenous microbial populations and for host health. How symbiotic relationships between hosts and native microbes persist during times of iron limitation is unclear. Here, we demonstrate that indigenous bacteria possess an iron-dependent mechanism that inhibits host iron transport and storage. Using a high-throughput screen of microbial metabolites, we found that gut microbiota produce metabolites that suppress hypoxia-inducible factor (HIF-2α) a master transcription factor of intestinal iron absorption and increase the iron storage protein ferritin, resulting in decreased intestinal iron absorption by the host. We identified 1,3-diaminopropane (DAP) and reuterin as inhibitors of HIF-2α via inhibition of heterodimerization. DAP and reuterin effectively ameliorated systemic iron overload. This work provides evidence of intestine/microbiota metabolic crosstalk that is essential for systemic iron homeostasis.

Graphical Abstract

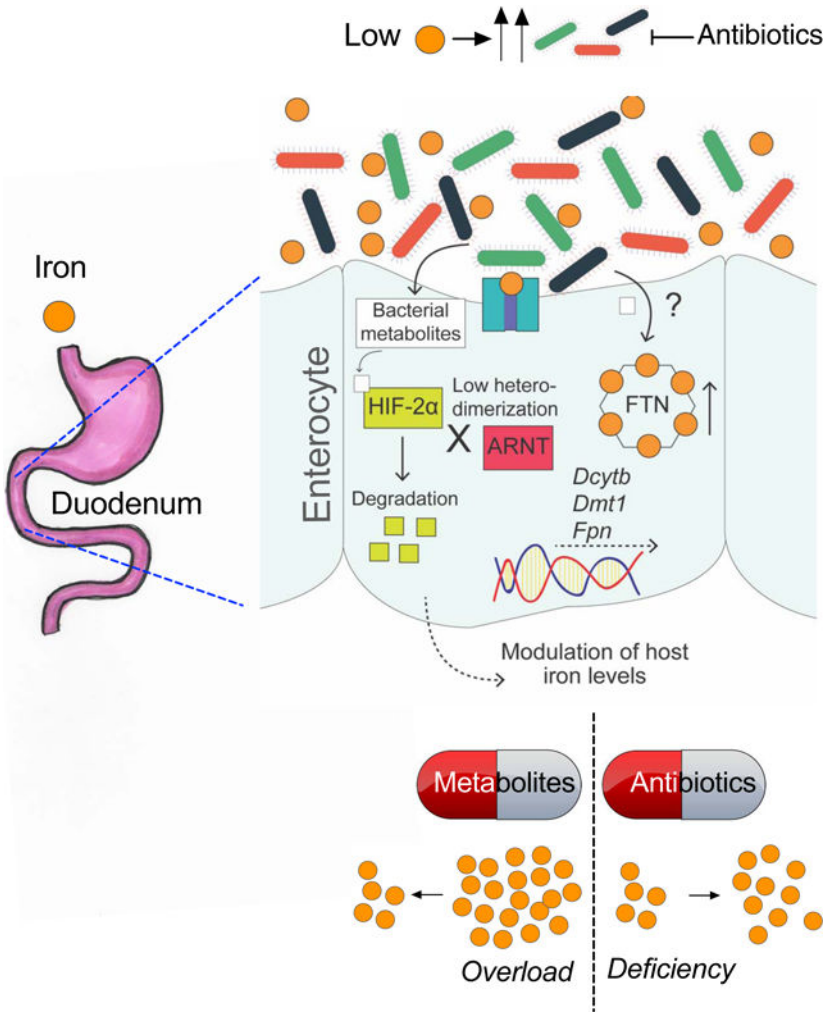

eTOC Blurb

Das et al. show that gut microbiota regulate host iron metabolism. Lactobacillus species are the major bacterial players involved in sensing intestinal iron levels and attenuating host iron absorption. The authors further show that mammalian iron disorders can be therapeutically targeted by modulating microbial species or their metabolites.

Introduction

Most organisms require iron to survive. Because of its unique redox chemistry, iron is critical for fundamental cellular biochemical processes. As both deficiency and excess of iron have deleterious effects, physiological iron homeostasis is tightly regulated. Mammalian iron acquisition is mediated by duodenal enterocytes via an integrative systemic and local regulatory system. Intestinal iron absorption is mainly regulated by hypoxia-inducible factor (HIF)-2α, an oxygen- and iron-regulated transcriptional factor that directly targets the three key intestinal iron transporters: divalent metal transporter 1 (DMT1), duodenal cytochrome b (Dcytb) and ferroportin (FPN)(Shah et al., 2009; Taylor et al., 2011). The importance of hypoxia signaling and the essentiality of HIF-2α in iron homeostasis have been highlighted in several genetic and pathophysiologic mouse models(Anderson et al., 2013; Das et al., 2015; Ramakrishnan et al., 2015; Xue et al., 2012). Ferritin (FTN), the major protein for cellular iron storage, acts as a source of bioavailable iron and as a detoxifying agent under conditions of cellular iron deficiency and excess, respectively(Harrison and Arosio, 1996). In addition, duodenal FTN regulates iron efflux into the circulation(Vanoaica et al., 2010). The hepatic hormone hepcidin, known as the master regulator of iron homeostasis, regulates iron flux in peripheral tissues by degrading FPN, the only known mammalian iron exporter. Recently, we showed that the hepcidin/FPN axis is essential for intestinal HIF-2α activation and proper response following an increase in iron demand (Schwartz et al., 2019).

The human intestine is host to a complex symbiotic microbial community. The intestinal microbiota relies on host factors and resources for survival and in turn is closely linked to human health and disease (Lin and Zhang, 2017; Martin et al., 2018; Pickard et al., 2017; Wang et al., 2011). Effective nutrient acquisition in the competitive environment of the human gut is essential for persistence of indigenous microbes. The importance of iron as a nutrient for microbial growth is well established and underscored by the association of iron with the growth and virulence of a wide range of pathogens(Constante et al., 2017; Jaeggi et al., 2015). Microbiota have evolved efficient strategies to acquire iron; however, it is not clear how they compete with their hosts for limited iron during times of nutrient scarcity. Moreover, the role of the microbiota in intestinal iron absorption and systemic iron homeostasis has not been studied.

In this study, we show that gut microbiota regulate systemic iron homeostasis in the host in two ways: by repressing intestinal iron-absorptive pathways via the inhibition of basal HIF-2α function, and by promoting cellular iron storage via the induction of FTN expression. Our results indicate that the host iron-sensing mechanism is intimately connected to and regulated by the gut microbiome. Intestinal iron deficiency leads to positive selection for a specific group of bacteria that produce metabolites that suppress HIF-2α and induce FTN. We identify two gut microbial metabolites, reuterin and 1,3

diaminopropane (DAP), that effectively suppress intestinal HIF-2α activity both *in vitro* and *in vivo*. Both of these metabolites prevent HIF-2α dimerization with aryl hydrocarbon receptor nuclear translocator (ARNT) and thus prevent tissue iron accumulation in a mouse model of iron overload.

Results

Gut microbiota restrict iron absorption by inhibiting HIF-2α expression.

To understand the role of gut microbiota in host systemic iron homeostasis, we assessed the hematological response of C57BL/6J germ-free (GF) mice to dietary iron restriction. Three groups of GF mice were fed different iron diets; enriched (350 ppm iron), sufficient (35 ppm iron), or deficient (<5 ppm iron); for 2 weeks and then compared with wild-type C57BL/6J specific pathogen-free (SPF) mice that were fed the same diets (Figure 1A). Complete Blood Count (CBC) analyses demonstrated that SPF mice that were fed the <5-ppm diet were more anemic than GF mice that were fed the same diet (Figure 1B). Interestingly, there was no difference in serum iron measurements between the SPF and GF mice across the dietary groups (Figure S1A). Compared with those in the respective SPF control mice, the liver and spleen iron levels were significantly lower in the GF mice that were fed the 350-ppm diet or the 35-ppm diet but significantly higher in the GF mice that were fed the <5-ppm diet (Figure S1A). These results imply that indigenous gut microbial populations are in competition with the host for iron, which becomes more apparent in iron-limited conditions.

We analyzed hepatic hepcidin mRNA expression to investigate the systemic response to iron deficiency in GF mice. Hepcidin expression in the GF mice showed iron-dependent downregulation similar to that in SPF mice (Figure S1B). Moreover, hepcidin expression in SPF mice that were given a broad-spectrum antibiotic cocktail (Abx) in their drinking water for 2 weeks were not significantly different than that in control mice that did not receive antibiotics (Figure S1C). The duodenum is the primary site for dietary iron absorption, and HIF-2α is the master regulator of intestinal iron homeostasis. HIF-2α is essential for the regulation of the apical transporters DMT1 and Dcytb as well as that of FPN(Shah et al., 2009) (Figure 1C). In conditions of high iron demand, mRNA expression of those transporters is induced as part of a feedback mechanism(Shah et al., 2009; Taylor et al., 2011). *Dmt1* and *Dcytb* mRNA levels were induced by dietary iron deficiency in SPF mice (Figure 1D). Furthermore, *Dmt1* and *Dcytb* expression levels were highly potentiated in iron-deficient GF mice (Figure 1D). *Dmt1* and *Dcytb* expression levels in GF mice were also significantly higher in the basal iron conditions (350-ppm and 35-ppm diets) compared to the respective SPF cohorts (Figure S1D and S1E).

To confirm the role of the gut microbiota in the regulation of *Dmt1* and *Dcytb* expression, GF mice on 350 ppm iron diet were conventionalized with the gut microbiota from healthy SPF mice on the same diet (GF-conv) given by a single oral gavage of fecal suspension (Figure 1E). GF-conv mice exhibited a significantly lower CBC values than the GF cohort (Figure S1F). The *Dmt1* and *Dcytb* mRNA levels in the GF-conv mice were also significantly lower than those in GF controls and were comparable to those in SPF mice (Figure 1F). To further confirm the role of the gut microbiota in the expression of *Dmt1* and *Dcytb*, SPF mice on standard chow diet (containing 270-ppm iron) were given Abx in

drinking water for 2 weeks to deplete their gut microbiota. The levels of *Dmt1* and *Dcytb* mRNA expression were significantly higher in the Abx-treated mice than in control mice that were not given Abx (Figure 1G). It is important to note here that Abx treatment resulted in a lower induction in *Dmt1* and *Dcytb* mRNA expression compared to what is observed in GF mice, most likely due to relatively very brief exposure of Abx to the host gut. Iron deficiency only regulates iron-related HIF-2α target genes and has no regulatory effect on proinflammatory or angiogenic genes(Schwartz et al., 2019). Consistent with that, GF mice did not demonstrate an increase in HIF-2α-dependent proinflammatory mediators (*Tnfa*, *Cxcl1*, *Ccl20*, *Il1β*, and *Steap4*) in response to iron deficiency. Moreover, there was no significant difference in the expression of HIF-2α-independent iron-related genes (transferrin receptor 1 (*Tfr1*), lipocalin2 (*Lcn2*), and hephastin (*heph*)) between GF mice and SPF mice (Supplementary Table 1). Interestingly, ankyrin repeat domain 37 (*Ankrd37*), a well-known but less-characterized HIF target,(Benita et al., 2009) and *Arnt*, the heterodimeric partner of the HIF-α subunit, were further induced in iron-deficient GF mice (Supplementary Table 1). In addition, the gut microbiota did not alter the expression of iron-regulatory genes in peripheral tissues (Supplementary Table 1). To confirm the involvement of HIF-2α in the gut microbiota-mediated regulation of intestinal iron transporters, mice with a disruption of HIF-2α specifically in intestinal epithelial cells ($Hif2\alpha^{\Delta IE}$) and their wild-type littermates ($Hif2\alpha^{F/F}$) were treated with Abx for 2 weeks. *Dmt1* and *Dcytb* expression was significantly induced in the $Hif2\alpha^{F/F}$ mice, but the effect was completely abolished in the $Hif2\alpha^{\Delta IE}$ mice (Figure 1H). Immunohistochemical analysis of GF duodenal epithelia revealed robust HIF-2α expression, which was even higher than that was observed in intestine-specific VHL-deleted ($Vhl^{\Delta IE}$) duodenum, a well-established model of intestinal HIF overexpression(Taylor et al., 2011). Also, the conventionalization of GF mice reduced HIF-2α expression to levels observed in SPF mice (Figure 1I). Together, these results demonstrate that gut microbiota suppress basal HIF-2α expression and activity in the small intestine.

Microbial metabolites inhibit HIF-2α expression and function.

To explore the underlying mechanism of gut microbiota-mediated inhibition of HIF-2α expression and function, human pluripotent stem cells (hPSCs) were used to generate human intestinal organoids (HIO)(Finkbeiner et al., 2015), and a non-pathogenic commensal *Escherichia coli* strain was then microinjected into the HIO lumen (Figure S2A)(Hill et al., 2017). Contrary to our *in vivo* findings, we observed robust induction of HIF-2α expression in HIOs injected with live bacteria but not in HIOs injected with heat-inactivated bacteria (Figure S2B). Consistent with the observed upregulation of the HIF-2α protein, the RNA expression of the HIF-2α-target apical iron transporters *DMT1* and *DCYTB* was also robustly induced by live bacteria in HIOs (Figure S2C). Expression analysis of inflammatory genes such as *TNFα*, *IL1β*, *IL8*, *CXCL1*, *CXCL2*, and *CCL20* suggests that there was generalized induction of the HIF pathway in the HIOs (Figure S2D). This is consistent with previous studies demonstrating the role of microbiota in the establishment of the luminal oxygen gradient *in vivo*, suggesting a mechanism of intestinal HIF-2α repression that is independent of oxygen levels(Albenberg et al., 2014).

The HIO-microbiota co-cultures are informative of bacterial sensing pathways, but they are mostly devoid of hetero-cellular metabolite communication, as many of the abundant microbial metabolites are derived from the host diet(Shankar et al., 2017; Wikoff et al., 2009). To investigate the possible role of microbial metabolites in HIF-2α regulation, crude extracts were isolated from duodenal contents using methanol-H_2O (80:20 *v/v*) as described previously(Bennett et al., 2008) (Figure 2A) and used to treat HCT116 human intestinal epithelial cells for 16 hours, with or without treatment with deferoxamine (DFO; a well-known iron chelator) or hypoxia (1% O_2). DFO and hypoxia both induced HIF-2α expression that was repressed by the duodenal metabolite extracts (Figure 2B). These results suggest that the gut lumen harbors small metabolites that are responsible for attenuation of the HIF-2α response.

To explore the physicochemical properties of the gut extracts, organic and aqueous phases were isolated from both duodenal and cecal (feces) contents by methanol-chloroform-water extraction (Figure 2C). Since it has already been shown (Figure 2B) that duodenal extracts possess the HIF-2α inhibitory properties in iron deficient or hypoxic conditions, we tested the duodenal organic extracts in presence of DFO and observed that they inhibited HIF-2α induction in HCT116 cells in a dose-dependent manner (Figure 2D). Similar results were obtained from the fecal organic extracts (Figure 2E). The duodenal and fecal aqueous extracts had significantly less repressive activity than the organic extracts (Figure S2E and S2F). Moreover, the fecal organic extracts had no effect on DFO-induced HIF-1α expression in HCT116 cells (Figure S2G), confirming the HIF-2α-specific effects of the gut luminal extracts. To rule out the presence of any small protein or peptides, fecal organic extracts were subjected to trypsin digestion or heating at 95°C, neither of which abolished the HIF-2α-repressive function of the extracts (Figure 2F). To investigate whether the HIF-2α-inhibitory compounds in the gut extracts are microbial in origin, organic and aqueous phase extracts were isolated from GF and GF-conv mice. Strikingly, only the organic extracts of the GF-conv mice, but not that of the GF, downregulated the DFO-mediated HIF-2α induction, confirming that the HIF-2α-inhibitory compounds are microbial in origin (Figure 2G).

To further confirm the role of gut microbiota in HIF-2α function, *Dmt1* promoter activity was analyzed by HIF response element (HRE)-based luciferase (HRE-Luc) assay after transient HIF-2α overexpression in HCT116 cells followed by treatment with fecal extracts from SPF or GF mice (termed SPF-metabolites and GF-metabolites, respectively). Consistent with the protein expression data, the SPF-metabolites significantly inhibited HRE-Luc activity, whereas the GF-metabolites had no significant effect (Figure 2H). In a similar experiment, HRE-Luc activity was used to investigate the impact of gut microbiota on HIF-1α function. There was no significant difference between SPF-metabolites and GF-metabolites with regard to HIF-1α function (Figure S2H). To identify compounds that might be responsible for the inhibition of HIF-2α activity and function, we generated a library of the 66 most abundant gut microbial metabolites according to a recent study(Matsumoto et al., 2012) (Supplemental Table 2). These compounds and live and heat-killed bacterial components were screened on the basis of HRE-Luc activity assay in HCT116 cells. The screen identified 12 compounds that significantly inhibited HIF-2α. Further analysis revealed that 9 compounds were toxic at doses at or below the range of physiological

concentration in the gut lumen (Malo, 1994; Parsons and Shaw, 1983; Schott et al., 1983) (Figure 2I). Thus, we narrowed our search to three metabolites: butyrate, propionate, and DAP. Further dose-dependent analysis of these three compounds in HCT116, HT29, and SW480 cells confirmed that the compounds inhibit HIF-2α expression at the protein level (Figure 2J). The lowest effective doses of butyrate, propionate and DAP that inhibited HIF-2α *in vitro* were 0.5 mM, 2.5 mM and 5μM, respectively (Figure 2J). The minimal inhibitory concentration of butyrate exceeded what is observed in the duodenum, whereas that of propionate and DAP were within the physiological range (Figures S3A and S3B). Butyrate and propionate are well characterized microbial metabolites present in mouse and human, but DAP has not been assessed rigorously. We now show that DAP was detected in both human and mouse guts in comparable concentrations (Figures S3B). Although DAP is detected in the GF mouse gut (Duodenum: ≦4μM; Colon: ≦10μM), its concentration increased by several folds following conventionalization (>5-fold in the duodenum:25μM; ≦10-fold in the colon:100≦μM), demonstrating a microbial contribution (Figure S3C). Analogously, Abx treatment of wild type mice drastically decreased the DAP concentration (Figure S3D). Moreover, DAP treatment at a dose range of 0–50μM did not show any obvious signs of toxicity and did not significantly affect cell growth (Figure S3E). 1,2 diaminopropane (1,2 DAP), which is not microbially derived, did not alter HIF-2α expression (Figure S3F). Acetate, an abundant gut microbial metabolite, had only a marginal effect on HIF-2α suppression at concentrations in the physiological range (Figure S3A and S3G). Lactic acid, a major metabolite produced by lactobacilli, had no effect on HIF-2α expression in intestinal epithelial cell lines (Figure S3H). Moreover, DAP and propionate did not inhibit HIF-1α, whereas butyrate increased HIF-1α protein expression, in agreement with the previous publications (Fachi et al., 2019; Kelly et al., 2015) (Figures S3I, S3J and S3K). Together our results demonstrate that endogenous bacterially derived metabolites inhibit HIF-2α with a high level of specificity.

Microbial metabolites are essential for FTN expression.

A third integral component in the regulation of intestinal iron absorption and systemic iron homeostasis is the iron-storage protein FTN. In a previous study, intestinal FTN disruption led to an increase in iron absorption(Vanoaica et al., 2010). FTN expression in the GF duodenum was significantly lower than that in the SPF duodenum in basal iron conditions (350-ppm and 35-ppm iron diets), whereas in the liver and spleen the effect was more pronounced with the 35-ppm iron diet (Figure 3A). FTN expression in the duodenum, liver, and spleen was significantly reduced in antibiotic-treated mice (Figure 3H, left panel). Duodenal FTN expression rapidly returned to the basal level in GF-conv mice (Figure S4A). There was no significant change in *Ftn* mRNA expression in the GF duodenum, which rules out transcriptional regulation by gut microbiota (Figure S4B).

To explore further, we utilized a model of gut microbiota depletion by Abx treatment in several genetic mouse models. In intestine-specific HIF-2α knockout (*Hif2*$\alpha^{\Delta IE}$) mice, the Abx treatment decreased duodenal FTN protein expression, confirming that the regulation of FTN by gut microbiota is HIF-2α independent (Figure 3B). NCOA4 mediates lysosomal degradation of FTN by a process known as ferritinophagy(Mancias et al., 2014). NCOA4-deficient cells show increased FTN expression due to a lack of FTN processing. Upon Abx

treatment, the *Ncoa4*$^{-/-}$ duodenum showed a rate of FTN decrease similar to that in wild-type controls (Figure 3C). Similarly, Abx treatment decreased FTN expression in both *Tlr2,4*$^{-/-}$ mice and *Myd88*$^{-/-}$ mice, ruling out the involvement of major bacterial sensing pathways (Figure 3D and 3E).

We next investigated the effects of butyrate, propionate, and DAP on FTN regulation. Those metabolites did not cause significant change in basal or iron (ferric ammonium citrate (FAC))-induced FTN expression in intestinal epithelial cell lines (Figure S4C and S4D). To explore the possibility that a novel group of metabolites was involved, we utilized metabolites extracted from feces of healthy SPF mice. Interestingly, the crude metabolites were able to induce FTN expression in iron-stimulated intestinal epithelial cell lines in a dose-dependent manner (Figure 3F). To investigate the systemic effects of the metabolites, we introduced the metabolites into antibiotic-treated mice by intraperitoneal injection (Figure 3G). FTN expression in the duodenum, liver, and spleen increased in the mice that were treated with the metabolites, suggesting that novel, unidentified microbial metabolite(s) play a role in systemic FTN regulation (Figure 3H, right panel).

DAP suppresses iron deficiency-induced and antibiotic-induced HIF-2α activity by blocking HIF-2α heterodimerization.

Because DAP, butyrate, and propionate effectively inhibited HIF-2α expression and activity *in vitro*, we next asked if those metabolites had any role in the suppression of HIF-2α activity in an *in vivo* setting. Mice on the 350-ppm or <5-ppm iron diets were given DAP (2 g/L)(Salim et al., 2000) in drinking water for 2 weeks. The expression of the HIF-2α-target apical iron transporters *Dmt1* and *Dcytb* was robustly induced by iron deficiency, and DAP administration significantly attenuated the response (Figure 4A). In addition, antibiotic-induced HIF-2α expression and function were also abrogated following the administration of DAP (Figure 4B). Similar experiments were performed to assess butyrate and propionate, but those metabolites could not suppress HIF-2α function *in vivo* (Figure S5A and S5B). Analysis of *Hif2α* mRNA expression in HCT116 cells treated with fecal metabolites from GF, GF-conv, or SPF mice revealed no significant difference among the treatment groups (Figure S5C). Butyrate and propionate increased *Hif2α* mRNA expression in HCT116 cells while DAP treatment had no significant effect, demonstrating that gut microbiota-mediated HIF-2α inhibition is independent of mRNA changes. (Figure S5D).

The 5'-UTR of HIF-2α harbors an iron response element (IRE), rendering it amenable to iron-regulatory protein (IRP)-mediated translational inhibition(Sanchez et al., 2007). To determine if butyrate, propionate, or DAP inhibit HIF-2α via an IRE-dependent mechanism, we performed a HIF-2α-IRE-based luciferase assay in HCT116 cells. In contrast to their effects on HIF-2α protein expression, the metabolites strongly increased HIF-2α-IRE activity, ruling out the possibility of an IRE-dependent mechanism (Figure S5E). The PAS-B domain of HIF-2α contains a hydrophobic cavity, that resembles a ligand-binding pocket. PT2385 selectively with high affinity binds to this cavity and disrupts HIF-2α heterodimerization with ARNT(Wallace et al., 2016). Consistent with the literature, the disruption of HIF-2α heterodimerization by PT2385 also decreased the HIF-2α protein stability (Figure 4C)(Wallace et al., 2016). To determine if DAP inhibits HIF-2α by a

mechanism similar to that of PT2385, we performed co-immunoprecipitation assays to assess HIF-2α–ARNT heterodimerization (Figure 4D). In agreement with the literature, PT2385 completely abrogated the HIF-2α–ARNT interaction (Figure 4E)(Chen et al., 2016; Cho et al., 2016). DAP also significantly inhibited the HIF-2α–ARNT interaction, although not to the extent of PT2385 (Figure 4E). To further verify the effect of DAP on the HIF-2α–ARNT interaction, we utilized a mammalian two-hybrid system (Figure 4F). Consistent with the co-immunoprecipitation results, DAP inhibited the Hif2α–ARNT interaction in the two-hybrid system (Figure 4G). It was recently reported that treatment with allosteric PT inhibitors decreases clear-cell renal carcinoma growth; however, long-term treatment led to resistance via missense mutations (S304M and G323E) in the ligand-binding cavity of HIF-2α (Chen et al., 2016; Cho et al., 2016). We generated double mutants of mouse HIF-2α (S305M and G324E; Figure 4H) and performed HRE-luciferase assays to assess the effect of the mutations on DAP-mediated HIF-2α inhibition. Indeed, the mutations in the PT-binding sites completely rescued the inhibition (Figure 4I). Together, these data suggest that bacterial metabolites have the ability to act as endogenous ligands for HIF-2α that suppress activity.

Limiting iron levels lead to more potent HIF-2α inhibition by microbial metabolites.

To understand how the production of microbial metabolites is integrated with host iron sensing, we asked if dietary iron manipulation could modulate the HIF-2α-suppressive function of microbial metabolites. HCT116 cells were treated with fecal metabolites extracted from mice that had received 350-ppm, 35-pmm, or <5-ppm iron diets for 2 weeks (Figure 5A). The metabolites isolated from the iron-deficient feces (<5-ppm) caused the most potent HIF-2α inhibition (Figure 5B). That suggests that iron deficiency selectively favors the growth or production of microbes and metabolites that exert relatively high levels HIF-2α inhibition. However, there was no change in DAP concentration in iron-deficient mice (Figures 5C). In addition, iron deficiency rather decreased the gut concentration of butyrate and did not alter acetate and propionate levels (Figure S6A).

Given the tendency of iron deficiency to lead to the production of metabolites that inhibit HIF-2α, and no change in DAP levels in iron-deficient guts, we next focused on the identification of other metabolites that can inhibit HIF-2α or are integrated with iron sensing. We first assessed changes in microbial communities due to luminal iron limitation (Figures 5D and 5E). Bacterial community analysis by 16S rRNA-encoding gene amplicon sequencing revealed *Lactobacillales* as the only bacterial genus showing robust increase in relative abundance in response to iron limitation in both duodenal contents and feces (Figure 5F and 5G). We have analyzed a total of five different lactobacillus species and among them the relative abundance of both *Lactobacillus johnsonii* and *Lactobacillus reuteri* were both significantly increased in the duodenal contents and feces following iron deficiency (Figure 5H, 5I and S6B). Also, a human isolate of *L. reuteri* showed increased abundance with increasing concentrations of DFO, whereas *E. coli* showed less abundance in the same conditions (Figure S6C). We were able to detect lactobacilli and specifically *L. reuteri* in the duodenal aspirates from healthy humans (Figures S6D and S6E). Together, these data suggest that limiting iron level favors the growth of a specific bacterial population, which might be producing metabolite(s) responsible for intestinal HIF-2α suppression.

Intestinal reuterin suppresses HIF-2α activity via blocking heterodimerization.

Reuterin (3-hydroxypropionaldehyde) is produced by *L. reuteri*, and little is known about its role in gut physiology other than its role as an antimicrobial compound(Schaefer et al., 2010) (Figure 6A). To produce reuterin, *L. reuteri* relies on a glycerol dehydratase-dependent metabolism of glycerol, which is only seen in bacteria(Chen and Chen, 2013). Reuterin is mostly undetected in the germ-free gut and its concentration robustly increased following conventionalization (Figure 6B). Analogously, Abx treatment drastically brought down the intestinal reuterin concentrations (Figure S7A). Physiological reuterin levels range from 250 μM in the proximal small intestine to greater than 1 mM in the colon (Figure 6C). Reuterin levels were robustly increased in mice that received a <5-ppm iron diet for 2 weeks compared with those in mice that received a 350-ppm iron diet (Figure 6C). Reuterin treatment led to a dose-dependent decrease of HIF-2α (but not HIF-1α) expression and activity in human intestinal epithelial cell lines (Figures 6D, 6E, S7B, and S7C). Similar to DAP, reuterin significantly disrupted HIF-2α–ARNT interaction (Figure 6F). HRE-Luc assay with the PT-binding-mutant sites of HIF-2α showed complete reversal of reuterin-mediated inhibition (Figure 6G).

Treatment with probiotics or antibiotic improved iron-related disorders in mouse models.

Given the *in vitro* and *in vivo* findings with our two novel HIF-2α-specific inhibitors, DAP and reuterin, we next asked whether those inhibitors could play any therapeutic roles in iron-overload disorders. The most common cause of iron-overload disorders is dysregulation of the hepcidin-FPN axis. We developed a temporal model of iron overload in a tamoxifen-inducible hepatic hepcidin knockout mouse model ($Hamp^{\Delta Liv}$)(Schwartz et al., 2019). The knockout mice showed rapid tissue accumulation of iron as early as 4 weeks following tamoxifen treatment (Figure 7A)(Schwartz et al., 2019). We provided DAP or *L. reuteri* probiotic suspension (as source of reuterin) in drinking water to $Hamp^{\Delta Liv}$ mice for 2 weeks prior to and for 2 more weeks following tamoxifen injection. Sufficient *L. reuteri* growth during the probiotic treatment was confirmed by bacteria-specific PCR using fecal DNA, showing that the size of the *Lactobacilli* population increased by about 25-fold (Figure S7D). Treatment with *L. reuteri* probiotic resulted in a robust production of reuterin in the intestine (Figure S7E). Quantitative iron assays revealed that the DAP treatment caused significant decreases in iron levels in the liver, pancreas, and heart in $Hamp^{\Delta Liv}$ mice compared with the levels in DAP-treated wild-type controls ($Hamp^{fl/fl}$), whereas *L. reuteri* probiotic treatment caused significant decreases in the pancreas and heart, but not in the liver (Figure 7B). We previously showed that temporal disruption of hepatic hepcidin activates intestinal HIF-2α(Schwartz et al., 2019). Western analysis showed a robust increase in the levels of HIF-2α-dependent intestinal iron transporters (DMT1, Dcytb, and FPN) in vehicle-treated $Hamp^{\Delta Liv}$ mice compared with those in wild-type control mice. That response was abrogated in $Hamp^{\Delta Liv}$ mice that were treated with DAP or *L. reuteri* probiotic (Figure 7C). In contrast, activation of HIF-2α would lead to increase intestinal iron absorption and treat anemic disorders. Since reuterin and DAP levels are observed in the small intestine and can be significantly decreased by Abx intervention to inhibit commensals and/or HIF-2α-suppressive metabolites may improve anemia. To determine if antibiotics would provide any benefit in anemic mouse models, rifaximin was assessed. Rifaximin is a gut-specific antibiotic due to its poor absorption when taken orally(Ma et al., 2007). Rifaximin did not

activate HIF-2α or chelate iron in cell lines (Figure S7F and S7G). Rifaximin treatment decreased both *L. johnsonii* and *L. reuteri* (Figure S7H) and increased the expression of iron-absorptive genes in mouse models of iron-deficient anemia (Figure 7D). Although hematocrit and hemoglobin values did not improve following 2-weeks of rifaximin treatment, there was significant increase in mean corpuscular hemoglobin (MCH) and mean corpuscular hemoglobin concentrations (MCHC) indicating an increase in RBC hemoglobinization. Increase in MCH is a reliable and early indicator of improvement of iron deficiency, a significant change usually occurs within a week's intervention.(Goddard et al., 2011) (Figures 7E and S7I). Overall, our results show that microbiome-based therapeutics can be used to successfully treat iron-related disorders.

Discussion

In this study, we showed that gut microbial metabolites regulate host systemic iron homeostasis by suppressing intestinal HIF-2α activity and by upregulating FTN expression. We identified two HIF-2α-inhibitory microbial metabolites that effectively prevent tissue iron accumulation in a mouse model of systemic iron overload. This is the first investigation that offers mechanistic insight into the crosstalk between the host and the indigenous microbiota with regard to systemic iron homeostasis.

GF mice exhibited significant resistance to anemia following dietary iron restriction. Although this finding can be explained from the perspective of host-microbe competition, there was no significant difference in the hepcidin response between GF livers and control livers. This suggests that gut microbiota regulate host iron metabolism via a hepcidin-independent mechanism. Dietary iron deficiency in GF mice led to an unprecedented induction of HIF-2α-target intestinal iron transporters, which was reproducible in an Abx-induced microbiota-depletion model. Consistent with those results, introduction of gut microbiota to GF mice was sufficient to restore basal levels of the intestinal iron transporters. While our *in vitro* organoid model failed to replicate the HIF-2α-suppressive effect of the gut bacteria, we inquired whether that finding might be attributable to a microbial function that is intimately associated with host systemic homeostasis. Recently, there has been renewed interest in elucidating the novel roles of microbial metabolites in host intestinal homeostasis. Of note, previous reports described the role of butyrate (the most abundant SCFA metabolite in the gut) in gut homeostasis by stabilization of HIF-1α(Fachi et al., 2019; Kelly et al., 2015). Gut extracts from only GF-conv (but not GF) mice were found to have HIF-2α inhibitory properties, highlighting the essential role of microbiota in such regulation. Using a high-throughput assay of HIF-2α activity to screen a library of highly abundant gut microbial metabolites, we identified several candidate HIF-2α inhibitors. Among them, DAP suppressed intestinal HIF-2α activity in at least two well-established mouse models of HIF-2α induction: dietary iron deficiency and antibiotic-induced microbiota depletion. DAP, a polyamine, is produced in the gut by several bacterial species(Chae et al., 2015). DAP is also known to be synthesized in the gut independent of microbiota(Matsumoto et al., 2017). Conventionalization of GF mice and Abx treatment reciprocally caused highly significant changes, strongly indicating that microbiota is the major contributor of intestinal DAP levels. Although DAP is reported to have iron-scavenging properties, its relationship with intestinal iron availability has never been

studied(Burrell et al., 2012). However, DAP was not shown to be integrated in host iron sensing. Bacterial community analysis revealed a robust increase in the intestinal abundance of genus *Lactobacillales* during dietary iron deficiency. At the species level, *L. johnsonii* and *L. reuteri* population (bacterial density relative to the total bacteria) were significantly induced by iron deficiency. It is important to note that while the relative *Lactobacillales* abundance and relative density of lactobacilli species were increased by iron-deficiency, their absolute densities in the corresponding gut lumen were not determined. Also, the gut concentration of reuterin, a product of *L. reuteri*, increased robustly during iron deficiency. Similar to DAP, reuterin was found to have HIF-2α-inhibitory properties. Both metabolites required the ligand binding pocket of HIF-2α for inhibition. The role of the hydrophobic cavity on HIF-2α was hitherto unknown, and therefore was termed a pseudo-ligand binding pocket. Our data suggest that selective bacterial metabolites are endogenous ligands that attenuate HIF-2α activity. It is important to note here that the gut extracts contain innumerable amounts of metabolites, many of their identities and functions are yet to be determined. So, the physiological HIF-2α inhibition following treatment with these pan-metabolite extracts is a collective and concerted effect, not necessarily only exerted by the metabolites identified in this work.

In agreement with previous reports we could successfully detect *L. reuteri* in human duodenum. Also, both DAP and reuterin were detected in human duodenum at similar levels to that of mice. Given the finding that gut levels of the reuterin and DAP can be effectively controlled by microbial presence (GF-conventionalization or Abx treatment), it strongly indicates that microbiota is the major source of these metabolites in the gut. It is important to note here that some of these metabolites (e.g. DAP) are also derived from dietary or environmental sources. In this work, we demonstrate that i) relevant bacterial population is present in both mouse and human guts, ii) their presence is necessary and sufficient for suppressing intestinal HIF-2α function, iii) the metabolites are also present in both mice and humans, iv) the duodenal concentrations of the metabolites are directly regulatable by gut bacterial colonization, and v) the duodenal concentration of reuterin is regulated by iron availability therein. However, we have not specifically pinpointed whether the metabolites detected in the duodenum are produced locally or originate more distally, e.g. from the cecum and the colon. Given the vastly higher density of bacteria in the cecum and the colon it is possible that the relevant metabolites are absorbed there into the portal circulation and redistributed to the proximal GI tract.

Our results clearly demonstrate that oral supplementation of DAP and reuterin results in a decrease in iron accumulation in mouse models of hemochromatosis, making this the first study to report the discovery of microbially derived metabolites with clinical relevance to iron-related disorders. Moreover, our results demonstrate an alternative or complementary mechanism by which gut bacteria compete for iron in addition to the known siderophoric acquisition systems. Currently the association between iron and bacterial reuterin and DAP pathways is unclear; however, DAP is reported to be a siderophore precursor for several bacteria, and several DAP pathway genes lie in close proximity to siderophore production operons(Burrell et al., 2012; Lynch et al., 2001).

The role of bacteria in FTN regulation was shown previously(Deschemin et al., 2016; Siegert et al., 2015). Consistent with those reports, our results show that native bacteria are essential in the regulation of local intestinal FTN. In addition, our results demonstrate that intestinal microbiota also play a role in peripheral-tissue FTN regulation. LPS, via activation of NFκB, is a known regulator of *Ftn* transcription in macrophages(Siegert et al., 2015). Our present results demonstrate a novel mechanism of FTN regulation, as there was no difference in *Ftn* mRNA levels between GF mice or Abx-treated mice and control mice. Moreover, host bacterial sensing pathways were not involved in FTN regulation by indigenous microbes. Our results show that a subset of metabolites other than HIF-2α suppressors regulate host iron-storage function by a novel yet unidentified mechanism. Bacterial metabolite-induced FTN expression provides an additional mechanism by which host iron absorption is decreased, leading to increased levels of luminal iron for resident bacteria. It is possible, however, that the systemic FTN response mediated by gut microbial metabolites reflects a mechanism to sequester iron from pathogens. Further studies are ongoing to identify FTN-regulatory metabolites and determine their physiological relevance.

There are no cures for hemochromatosis, and current maintenance therapies provide a benefit by decreasing tissue iron accumulation. The two mainstay therapies for hemochromatosis are iron chelators such as DFO and routine phlebotomy, but those therapies are slow acting with many off-target effects, leading to low patient adherence(Adams and Barton, 2007). Our results provide evidence that probiotics may be effective as a stand-alone or adjuvant therapy. Moreover, iron-deficiency anemia is a global health crisis affecting more than a billion people(Lopez et al., 2016). Oral iron supplementation is an effective treatment, but that approach is risky and can even be fatal, especially in third-world countries were infections are endemic(Jonker and Boele van Hensbroek, 2014). Antibiotics have been shown to be effective in improving anemia; however, the improvement was thought to be mainly due to a decrease in bacterial infections(Gifford et al., 2015; Gifford et al., 2012). We clearly demonstrate that antibiotics may have additional beneficial effects outside of pathogen control, specifically by increasing intestinal iron absorption.

In summary, our results demonstrate a previously undescribed mechanism of metabolic crosstalk between microbiota and the host intestinal epithelium that regulates intestinal and systemic iron homeostasis. We provide *in vivo* evidence that probiotics may play a beneficial role in diseases of iron overload, whereas antibiotics may be effective in iron deficiency

Limitations of study

Our data has utilized a mouse model and assessed the role of the microbiota in host nutrient absorption. The data demonstrates that DAP and reuterin are functional metabolites that modulate host iron absorption. These metabolites are also present in human duodenum.

However, we have not demonstrated that DAP and reuterin can inhibit HIF-2α activty in the context of a human microbiome. Similar to this limitation, we show that *Lactobacillus johnsonii* and *Lactobacillus reuteri* respond to changes in luminal iron, these changes have not been assessed in iron deficient or anemic patients. Additionally, as noted above, we have not identified the exact anatomical source of the gut microbial metabolites. They could be

produced more distally and by several different microbial species. It is not possible currently to determine if local or distal sources are responsible for the changes observed in the duodenum. Lastly, mouse models of iron-related disorders do not completely recapitulate the extent of the anemic or iron overload phenotype observed in humans, further pre-clinical studies are needed to determine if microbial-based therapies could have efficacy in patients.

STAR Methods

Lead Contact and Materials Availability

A new construct was generated in this study : Mouse HIF-2α mutant of two PT2399 binding sites (pCDNA3-HIF-2αG324E+S305M). And a new mouse line generated in this study : NCOA4$^{-/-}$. Further information and requests for resources and reagents should be directed to and will be fulfilled by the Lead Contact, Yatrik Shah (shahy@umich.edu). All unique/stable reagents generated in this study are available from the Lead Contact with a completed Materials Transfer Agreement.

Experimental Model and Subject Details

Mice—All mice used in this study were on a C57BL/6J background. Both male and female mice were used throughout and littermates were randomly assigned to experimental groups. The GF mice were housed in a temperature-controlled (21±1.1°C), barrier facility using individual Isocages ® (Tecniplast) in the University of Michigan Germ-Free Mouse Core. All other mice were housed in a temperature-controlled (21±1.1°C), specific-pathogen free (SPF) facility on a 12 h light/dark cycle and fed ad libitum with standard chow diet containing 270 ppm iron. For iron studies, mice were fed with iron enriched (350 ppm iron), iron sufficient (35 ppm iron) or low-iron (<5 ppm iron) chow for the 1–2 weeks. There was no significant gender differences with regards to their iron status as reported previously(Schwartz et al., 2019). NCOA4$^{-/-}$ mice were generated by the University of Michigan Transgenic Core using CRISPR-cas9 mediated targeting of exon 3 (guide RNA: 5'-AGAGGTGTGGCTCAATGAAC-3'). Intestine-specific HIF-2α knockout (*Hif2a*$^{\Delta IE}$:Vil^{Cre};*Hif2a*$^{F/F}$), intestine-specific VHL knockout (*Vhl*$^{\Delta IE}$: Vil^{Cre}; *Vhl*$^{F/F}$), liver-specific tamoxifen-inducible hepcidin knockout (*Hamp*$^{\Delta Liv}$:Alb^{CreERT2}; *Hamp*$^{F/F}$), *Tlr2/4*$^{-/-}$ and *Myd88*$^{-/-}$ mice were described previously(Eigenbrod et al., 2008; Schwartz et al., 2019; Shah et al., 2009). All animal studies were carried out in accordance with Association for Assessment and Accreditation of Laboratory Animal Care International guidelines and approved by the University Committee on the Use and Care of Animals at the University of Michigan.

Human Subjects—For detection of lactobacillus in the upper gastrointestinal tract of humans, duodenal aspirates were collected from 17 healthy subjects from a previously reported study group (Koenigsknecht et al., 2017). Physiological concentrations of 1,3 DAP and reuterin were determined from 10 subjects from the same group. The study is a part of clinical trial and was approved by the institutional review boards at the University of Michigan (IRBMED, protocol number HUM00085066) and the Department of Health and Human Services, Food and Drug Administration (Research Involving Human Subjects Committee/RIHSC, protocol number14–029D). The study was carried out in accordance

with the protocol and applicable local regulatory requirements. All subjects (both male and female, age 18–55 years) provided written informed consents and participated after completion of a physical examination and review of their previous medical history.

Method details

Cell culture and proliferation assays—Human intestinal cell lines HCT116, HT29 and SW480, and human embryonic kidney cells HEK293T were used. All cells were maintained in complete DMEM medium (supplemented with 10% fetal bovine serum and 1% antibiotic/antimycotic agent) at 37°C in 5% CO_2 and 21% O_2. For hypoxic experiments, cells were maintained in 1% O_2 in an enclosed humidified chamber by replacing the atmospheric air with a gas mixture comprising of 1% O_2, 5% CO_2 and 95% N_2. Growth assays were performed using MTT reagent (Thiazolyl Blue Tetrazolium Bromide). Briefly, cells were plated down and 24-hours following plating a Day 0 reading was taken. Cells were incubated for 45 minutes with MTT solution (5× concentrate stock: 5 mg/ml, in 1XPBS, pH 7.4). Media and MTT solution were then carefully aspirated followed by solubilization with dimethyl sulfoxide. Absorbance was read at 570nm. Following the Day 0 read, the cells were treated with different doses of DAP doses and readings were taken after 24-hours.

HIO culture and microinjection with bacteria—Differentiated human intestinal organoid (HIO)s were generated from human pluripotent stem cell (hPSC)s, maintained and used for microinjection with commensal bacterial culture as described previously (Hill et al., 2017). HIOs were maintained in media containing EGF, Noggin, and R-spondin (ENR media) in 60 μl Matrigel (8 mg/ml) without antibiotics prior to microinjection experiments. For hypoxia experiments, HIOs were put in a hydrated and sealed chamber filled with 1% O_2, 5% CO_2, and balance N_2 and maintained at 37°C for 16 hours. HIO microinjection with PBS, live- or heat killed *E. coli* were performed under microscopic guidance with the aid of thin wall glass capillaries (TW100F-4, World Precision Instruments) after shaping them with a P-30 micropipette puller (Sutter Instruments). After the microinjection, the HIO culture media was carefully aspirated and the wells were rinsed with sterile PBS and maintained in ENR media containing penicillin and streptomycin to remove any bacteria.

Bacterial strains—For HIO colonization and bacterial growth analysis, *E. coli* strain ECOR2 (ATCC 35321; Originally isolated from healthy adult stool sample, gift of Dr. Seth Walk, Montana State University) and *L. reuteri* strain MM4–1A (PTA5475, ATCC; Originally isolated from human breast milk, gift of Dr. Robert Britton, Baylor College of Medicine) were used as described previously (Hill et al., 2017). The bacteria were cultured in Luria broth (LB) media at 37°C under atmospheric oxygen concentration.

Antibiotics treatment—Antibiotics treatment (Abx) was performed as described previously(Ramakrishnan et al., 2019). Briefly, animals were given water containing antibiotic cocktail (Ampicillin 1 g/L, neomycin 1 g/L, gentamycin 500 mg/L; penicillin 100U/L) in the drinking water, ad libitum. In addition, oral gavage of vancomycin (1 mg/mL) and metronidazole (0.5 mg/mL) was given on alternate days for 1–2 weeks. Rifaximin was blended with <5-ppm iron diet and administered at 20 mg/kg body weight/day as described previously (Ma et al., 2007).

Metabolite supplementation—Sodium salts of butyrate and propionate were given in drinking water at 150mM and 100mM concentrations, respectively(Smith et al., 2013). 1,3 Diaminopropane was given in drinking water at a concentration of 2g/L(Salim et al., 2000). For reuterin supplementation of mouse gut, *L. reuteri* probiotic tablets containing *L. reuteri* DSM17938 probiotic strain (100 million CFU per tablet) was added in drinking water (1 tablet per 200 ml).

Hematological and iron analysis—CBC (complete blood count) analysis was performed by the Unit for Laboratory Animal Medicine Pathology Core at The University of Michigan. Serum and tissue nonheme iron was quantified as described previously (Anderson et al., 2013). Briefly, serum and homogenized tissues were processed in a 1M HCl and 10% (wt/ vol) trichloroacetic acid solution and heated for 1 h at 95°C. The samples were spun at 13,000 rpm, room temperature for 20 minutes, then the supernatant was incubated with an iron assay reagent ((1:1, 1mM ferrozine : 3M Sodium Acetate, pH 5.5) plus 1% mercaptoacetic acid) at 1:1 ratio until the color turns into purple. Iron quantitation was done at 562 nm and compared with iron standard solution (1 mg/ml Fe in 2% HNO_3).

Real-time quantitative PCR—1 μg of total RNA extracted using trizol reagent from mouse tissues (duodenal epithelial scrapes, liver and spleen), human intestinal cell lines and human intestinal organoid (HIO)s were reverse transcribed to cDNA using SuperScript™ III First-Strand Synthesis System (Invitrogen). Quantitative PCR (qPCR) reactions were set up in three technical replicates for each sample by combining equal concentration of cDNA, gene-specific forward and reverse primers, with SYBR green master mix, and run in QuantStudio 5 Real-Time PCR System (Applied BioSystems). The fold-change of the genes were calculated using the ΔΔCt method using β-actin as the housekeeping gene. The primers are listed in Supplementary Table 3.

DNA extraction from feces and bacteria-specific PCR—DNA from mouse feces was extracted by using DNeasy Blood and Tissue Kit. 0.5–1.0 ng of DNA was used for bacteria-specific PCR, relative abundance was determined after normalization with the readings from the value from PCR by pan-bacteria primers. The primers are listed in Supplementary Table 3.

Western blotting and co-immunoprecipitation—Whole-cell and membrane lysate preparations were described previously (Anderson et al., 2013). Whole-cell lysates were prepared from tissue or cell lines by RIPA buffer. Briefly, Cell or tissue homogenates were incubated in RIPA buffer for 15–20 minutes on ice followed by centrifugation at 13,000 rpm for 15 minutes at 4°C. Supernatants were transferred to a new tube and mixed with 5× Laemmli buffer and boiled for 5 min. Membrane lysate was prepared by dounce homogenization of scraped duodenal epithelia followed by passaging the samples through a 27-gauge needle 7–10 times in lysis buffer (5mM Tris pH 8.0, 2mM EDTA, 250mM of sucrose and protease inhibitor). The nuclei were pelleted at 1,000 × g for 10 minutes, and the supernatant was centrifuged at 45,000 × g for 45 minutes using Optima™ TLX Ultracentrifuge (Beckman). The resulting membrane pellet was resuspended in storage buffer (75mM Tris pH 8.0, 12.5mM $MgCl_2$, 5mM EDTA and protease inhibitor). Membrane

extracts were mixed with 2× Laemmli buffer and incubated at 42°C for 5 min. Co-immunoprecipitation experimental procedure was performed with GFP-Trap magnetic beads and is summarized in Figure 4D. Lysates containing 30–40 μg of protein per well were separated by SDS-PAGE, transferred onto nitrocellulose membranes, and immunoblotted overnight at 4°C with antibodies against HIF-2α, HIF-1α, FTH1, FPN, DMT1, DCYTB, ARNT, Actin and GAPDH. All the primary antibodies were used at a dilution of 1:1000. HRP-conjugated secondary antibodies used were: anti-rabbit anti-mouse and anti-goat at dilution of 1: 2000, and immunoblots were developed using chemidoc touch imaging system (ChemiDoc, BioRad).

Immunostaining—OCT-embedded frozen tissues were sectioned (6 μm) and fixed with PBS-buffered formalin for 15 min and permeabilized for 10 min using 0.05% Triton X-100. Sections were blocked in 5% (vol/vol) normal goat serum in TBST for 30 min at room temperature and probed with polyclonal rabbit anti–HIF-2α antibody (1: 100) overnight at 4°C. The samples were then incubated with rabbit IgG Alexa Fluor 594 (1: 500) for 1 hour in dark at room temperature, followed by mounting and counterstaining by Prolong™ Gold Antifade Mountant with DAPI.

Luciferase assay—Cells were seeded into a 24-well plate at a cell density of 5×10^4 cells per well. The luciferase constructs for HIF response element (HRE) and HIF-2α IRE were previously described (Sanchez et al., 2007; Shah et al., 2009). The luciferase constructs were co-transfected with oxygen stable HIF-2α, HIF-1α or empty vector (EV) into cells with polyethylenimine. To screen the most abundant gut microbial metabolites for HIF-2α inhibition, a DMT1 promoter luciferase construct harboring HIF response elements (HRE) (hereafter referred to as HRE-Luc) was performed in HCT116 cells. We narrowed our search to metabolites that generated statistically significant ($p < 0.05$) inhibition of HRE-Luc activity by 0.3-fold or greater. To investigate the role of indicated metabolites in HIF-2α-ARNT interaction, pG5 luciferase vector was co-transfected with pBIND-HIF-2α and pACT-ARNT into cells using the protocol described in CheckMate™ Mammalian Two-Hybrid System (Promega). To identify the mechanism how indicated metabolites influenced HIF-2α-ARNT interaction, two PT2399 binding sites in the mouse HIF-2α was mutated to generate mHIF-2αG324E+S305M and HRE luciferase assay was performed. Cells were lysed in reporter lysis buffer, and firefly luciferase activity was measured using Synergy™ 2 Multi-Mode Microplate Reader (BioTek) and normalized to β-galactosidase (β-gal) activity 48 hours after transfection.

Metabolite extraction—Metabolites from mouse duodenal contents and feces were extracted by two methods. First, crude metabolites were extracted by 80% methanol [methanol: water (80:20; v/v)] extraction as described previously (Bennett et al., 2008). Briefly, pre-weighed freshly collected sample were homogenized in 3–5 ml of dry ice-cold 80% methanol and incubated in dry ice for 10 minutes followed by centrifugation at 4,000 rpm for 10 minutes at 4°C. Supernatant was passed through a 70-μm cell strainer to get rid of the debris and centrifuged again at 13,000 rpm for 10 minutes at 4°C. Supernatant was then transferred to a new sample tube and subjected to Speedvac (Eppendorf Vacufuge) to obtain a metabolite pellet. Second, for physicochemical characterization, metabolites were

extracted in organic and aqueous phases using methanol-chloroform-water extraction method as described previously (Sridharan et al., 2014). Briefly, 3–5 ml of dry ice-cold methanol/chloroform (2:1, v/v) was added to a sample tube containing a pre-weighed freshly collected sample. After homogenization on ice, the sample tube was centrifuged at 13,000 rpm for 10 min at 4°C. The supernatant was then transferred to a new sample tube through a (70-μm) cell strainer. In a dry ice-cold sample tube, 0.6 ml of ice-cold water was added to 1.5 ml of supernatant, the sample tube was vortexed vigorously for 30 seconds and centrifuged at 13,000 rpm for 10 min at 4°C to obtain phase separation. The upper and lower phases were separately collected into fresh sample tubes without disturbing the interface, followed by Speedvac procedure. The metabolite pellets were suspended in DMSO and corn oil (5 mg/100 μl) for *in vitro* experiments and *in vivo* intraperitoneal injections, respectively.

16S rRNA gene sequencing and bacterial community analysis—Bacterial sequencing analysis was done as described previously at the Microbial Systems Molecular Biology Lab, a part of the University of Michigan Host Microbiome Initiative (Ramakrishnan et al., 2019). Briefly, the V4 region of the 16S rRNA gene was amplified from the mouse duodenal contents or feces using the Dual-indexing sequencing strategy. Sequencing was done on the Illumina MiSeq platform, using a MiSeq Reagent Kit V2 500 cycles, according to the manufacturer's instructions with modifications. Bacterial community analysis was done based on Mothur wiki.

Gas chromatography-mass spectrometry analysis of metabolites

Extraction and derivatization method for DAP: 10 mg of sample was mixed with 150 μL of 6% TCA solution (containing 10 μg/mL 2,3-$^{13}C_2$ Alanine), homogenized at 6500 rmp, 25 s, with 1.0 mm diameter beads added and then centrifuged at 20,000 RCF for 10 min at 4°C, the supernatant liquor was collected in glass vial and mixed with 300 μL 50mM Sodium hydroxide solution and 300 μL propanol/pyridine (v:v=3:2). 100 μL of propylchloroformate subsequently was added on ice following a vortex for 1 min. The samples were derivatized in an incubator at 35°C for 30 min. The derivatized samples were extracted with 75 μL of hexane twice, then a total of 150 μL of extracts was obtained and stored at 4°C for GC-MS analysis.

Extraction and derivatization method for reuterin: 10 mg of sample was mixed with 5 μL of 1 mM 2,2,4,4 - D_4 citric acid and 500 μL of cold 80% methanol, homogenized at 6500 rmp, 25 s, with 1.0 mm diameter beads added. 200 μL each of cold water and chloroform are added and homogenized again followed by centrifuging at 20,000 RCF for 10 min at 4°C, the supernatant liquor was collected and transferred into 1.8 mL glass vial and dry down in vacuum speeder. The dried sample was mixed with each 50 μL pyridine and MSTFA followed by a vortex for 5 min, the samples were derivatized in −20°C refrigerator overnight. Glass vial containing sample was sonicated for 30 min and then centrifuged at 20,000 RCF for 10 min at 4°C, supernatant liquor was collected and stored at 4°C for GC-MS analysis.

GC-MS method: For DAP, a headspace sampler was utilized, for reuterin a standard GC/MS sampling was performed. A HP5 ms (5%Phenylmethylpolysiloxane) capillary GC

column (30 m × 250 μm i.d. 0.25 μm film thickness, Agilent Technologies) was employed with helium as the carrier gas at a constant flow rate of 1 mL/min. The initial column oven temperature was 70°C for 2 min and then increased to 230°C at a rate of 20°C/min. The temperatures of the front inlet, transfer line and mass source were set at 250°C, 280°C, and 230°C, respectively. The total run time was 20 min and the mass spectral data was collected in full scan mode with a mass range 30–400 m/z. injection volume is 1 μL. 2,2,4,4 - D_4 citric acid and reuterin were quantified by peak areas of extracted m/z 276 (Ghassempour et al., 2004) and m/z 219 (Talarico and Dobrogosz, 1989), respectively as described previously. Analysis of intestinal SCFAs was done as described previously (Cai et al., 2017).

Quantification and Statistical analysis

Main *in vitro* experiments were validated by multiple cell lines. Each cell line experiment was performed with duplicate or triplicates for each condition and repeated at least three times to ensure reproducibility. Blinding was performed whenever deemed to be appropriate and applicable. Sample description and identification was unavailable to the core personnel during data plotting and analyses. No sample or data was excluded from the study for statistical purposes. Statistical details of all experiments can be found in the figure legends. The sample numbers are mentioned in the figures and denote biological replicates unless otherwise noted. Results are expressed as the mean ± SEM. Significance between 2 groups was tested using a 2-tailed, unpaired *t* test. Significance among multiple groups was tested using a one-way ANOVA followed by Tukey's post hoc test. GraphPad Prism 7.0 was used to conduct the statistical analyses. Statistical significance is described in the figure legends as: * $P < 0.05$, ** $P < 0.01$, *** $P < 0.001$.

Data and code availability

The 16S rRNA gene sequencing data of duodenal and fecal microbiota from mice fed with different iron diets have been deposited in NCBI BioProject (ID: PRJNA576605).

Supplementary Material

Refer to Web version on PubMed Central for supplementary material.

Acknowledgements

This work was supported by NIH grants (CA148828 and DK095201 to Y.M.S), F31 DK11655 to A.J.S., The University of Michigan Center for Gastrointestinal Research (DK034933), a pilot grant from the University of Michigan GI Spore (CA130810 to Y.M.S.), The University of Michigan Microbiome Explorer Program, NIAID Novel Alternative Model Systems for Enteric Diseases (NAMSED) consortium (U19AI116482 to J.R.S. and V.B.Y), Crohn's & Colitis Foundation Senior Research Award (410234) to N.I., Spanish Ministry of Science Innovation and Universities (RTA2017-00002-00-00 to J.L.A.).

References

Adams PC, and Barton JC (2007). Haemochromatosis. Lancet 370, 1855–1860. [PubMed: 18061062]

Albenberg L, Esipova TV, Judge CP, Bittinger K, Chen J, Laughlin A, Grunberg S, Baldassano RN, Lewis JD, Li H, et al. (2014). Correlation between intraluminal oxygen gradient and radial partitioning of intestinal microbiota. Gastroenterology 147, 1055–1063 e1058. [PubMed: 25046162]

Anderson ER, Taylor M, Xue X, Ramakrishnan SK, Martin A, Xie L, Bredell BX, Gardenghi S, Rivella S, and Shah YM (2013). Intestinal HIF2αlpha promotes tissue-iron accumulation in

disorders of iron overload with anemia. Proc Natl Acad Sci U S A 110, E4922–4930. [PubMed: 24282296]

Benita Y, Kikuchi H, Smith AD, Zhang MQ, Chung DC, and Xavier RJ (2009). An integrative genomics approach identifies Hypoxia Inducible Factor-1 (HIF-1)-target genes that form the core response to hypoxia. Nucleic Acids Res 37, 4587–4602. [PubMed: 19491311]

Bennett BD, Yuan J, Kimball EH, and Rabinowitz JD (2008). Absolute quantitation of intracellular metabolite concentrations by an isotope ratio-based approach. Nat Protoc 3, 1299–1311. [PubMed: 18714298]

Burrell M, Hanfrey CC, Kinch LN, Elliott KA, and Michael AJ (2012). Evolution of a novel lysine decarboxylase in siderophore biosynthesis. Mol Microbiol 86, 485–499. [PubMed: 22906379]

Cai J, Zhang J, Tian Y, Zhang L, Hatzakis E, Krausz KW, Smith PB, Gonzalez FJ, and Patterson AD (2017). Orthogonal Comparison of GC-MS and (1)H NMR Spectroscopy for Short Chain Fatty Acid Quantitation. Anal Chem 89, 7900–7906. [PubMed: 28650151]

Chae TU, Kim WJ, Choi S, Park SJ, and Lee SY (2015). Metabolic engineering of Escherichia coli for the production of 1,3-diaminopropane, a three carbon diamine. Sci Rep 5, 13040. [PubMed: 26260768]

Chen G, and Chen J (2013). A novel cell modification method used in biotransformation of glycerol to 3-HPA by Lactobacillus reuteri. Appl Microbiol Biotechnol 97, 4325–4332. [PubMed: 23359000]

Chen W, Hill H, Christie A, Kim MS, Holloman E, Pavia-Jimenez A, Homayoun F, Ma Y, Patel N, Yell P, et al. (2016). Targeting renal cell carcinoma with a HIF-2 antagonist. Nature 539, 112–117. [PubMed: 27595394]

Cho H, Du X, Rizzi JP, Liberzon E, Chakraborty AA, Gao W, Carvo I, Signoretti S, Bruick RK, Josey JA, et al. (2016). On-target efficacy of a HIF-2alpha antagonist in preclinical kidney cancer models. Nature 539, 107–111. [PubMed: 27595393]

Constante M, Fragoso G, Lupien-Meilleur J, Calve A, and Santos MM (2017). Iron Supplements Modulate Colon Microbiota Composition and Potentiate the Protective Effects of Probiotics in Dextran Sodium Sulfate-induced Colitis. Inflamm Bowel Dis 23, 753–766. [PubMed: 28368910]

Das N, Xie L, Ramakrishnan SK, Campbell A, Rivella S, and Shah YM (2015). Intestine-specific Disruption of Hypoxia-inducible Factor (HIF)-2alpha Improves Anemia in Sickle Cell Disease. J Biol Chem 290, 23523–23527. [PubMed: 26296885]

Deschemin JC, Noordine ML, Remot A, Willemetz A, Afif C, Canonne-Hergaux F, Langella P, Karim Z, Vaulont S, Thomas M, et al. (2016). The microbiota shifts the iron sensing of intestinal cells. FASEB J 30, 252–261. [PubMed: 26370847]

Eigenbrod T, Park JH, Harder J, Iwakura Y, and Nunez G (2008). Cutting edge: critical role for mesothelial cells in necrosis-induced inflammation through the recognition of IL-1 alpha released from dying cells. J Immunol 181, 8194–8198. [PubMed: 19050234]

Fachi JL, Felipe JS, Pral LP, da Silva BK, Correa RO, de Andrade MCP, da Fonseca DM, Basso PJ, Camara NOS, de Sales ESEL, et al. (2019). Butyrate Protects Mice from Clostridium difficile-Induced Colitis through an HIF-1-Dependent Mechanism. Cell Rep 27, 750–761 e757. [PubMed: 30995474]

Finkbeiner SR, Freeman JJ, Wieck MM, El-Nachef W, Altheim CH, Tsai YH, Huang S, Dyal R, White ES, Grikscheit TC, et al. (2015). Generation of tissue-engineered small intestine using embryonic stem cell-derived human intestinal organoids. Biol Open 4, 1462–1472. [PubMed: 26459240]

Ghassempour A, Nojavan S, Talebpour Z, Amiri AA, and Najafi NM (2004). Monitoring of the fermentation media of citric acid by the trimethylsilyl derivatives of the organic acids formed. J Agric Food Chem 52, 6384–6388. [PubMed: 15478996]

Gifford AH, Dorman DB, Moulton LA, Helm JE, Griffin MM, and MacKenzie TA (2015). Serum Iron Level Is Associated with Time to Antibiotics in Cystic Fibrosis. Clin Transl Sci 8, 754–758. [PubMed: 26643575]

Gifford AH, Moulton LA, Dorman DB, Olbina G, Westerman M, Parker HW, Stanton BA, and O'Toole GA (2012). Iron homeostasis during cystic fibrosis pulmonary exacerbation. Clin Transl Sci 5, 368–373. [PubMed: 22883617]

Goddard AF, James MW, McIntyre AS, Scott BB, and British Society of G (2011). Guidelines for the management of iron deficiency anaemia. Gut 60, 1309–1316. [PubMed: 21561874]

Harrison PM, and Arosio P (1996). The ferritins: molecular properties, iron storage function and cellular regulation. Biochim Biophys Acta 1275, 161–203. [PubMed: 8695634]

Hill DR, Huang S, Nagy MS, Yadagiri VK, Fields C, Mukherjee D, Bons B, Dedhia PH, Chin AM, Tsai YH, et al. (2017). Bacterial colonization stimulates a complex physiological response in the immature human intestinal epithelium. Elife 6.

Jaeggi T, Kortman GA, Moretti D, Chassard C, Holding P, Dostal A, Boekhorst J, Timmerman HM, Swinkels DW, Tjalsma H, et al. (2015). Iron fortification adversely affects the gut microbiome, increases pathogen abundance and induces intestinal inflammation in Kenyan infants. Gut 64, 731–742. [PubMed: 25143342]

Jonker FA, and Boele van Hensbroek M (2014). Anaemia, iron deficiency and susceptibility to infections. J Infect 69 Suppl 1, S23–27. [PubMed: 25264159]

Kelly CJ, Zheng L, Campbell EL, Saeedi B, Scholz CC, Bayless AJ, Wilson KE, Glover LE, Kominsky DJ, Magnuson A, et al. (2015). Crosstalk between Microbiota-Derived Short-Chain Fatty Acids and Intestinal Epithelial HIF Augments Tissue Barrier Function. Cell Host Microbe 17, 662–671. [PubMed: 25865369]

Koenigsknecht MJ, Baker JR, Wen B, Frances A, Zhang H, Yu A, Zhao T, Tsume Y, Pai MP, Bleske BE, et al. (2017). In Vivo Dissolution and Systemic Absorption of Immediate Release Ibuprofen in Human Gastrointestinal Tract under Fed and Fasted Conditions. Mol Pharm 14, 4295–4304. [PubMed: 28937221]

Lin L, and Zhang J (2017). Role of intestinal microbiota and metabolites on gut homeostasis and human diseases. BMC Immunol 18, 2. [PubMed: 28061847]

Lopez A, Cacoub P, Macdougall IC, and Peyrin-Biroulet L (2016). Iron deficiency anaemia. Lancet 387, 907–916. [PubMed: 26314490]

Lynch D, O'Brien J, Welch T, Clarke P, Cuiv PO, Crosa JH, and O'Connell M (2001). Genetic organization of the region encoding regulation, biosynthesis, and transport of rhizobactin 1021, a siderophore produced by Sinorhizobium meliloti. J Bacteriol 183, 2576–2585. [PubMed: 11274118]

Ma X, Shah YM, Guo GL, Wang T, Krausz KW, Idle JR, and Gonzalez FJ (2007). Rifaximin is a gut-specific human pregnane X receptor activator. J Pharmacol Exp Ther 322, 391–398. [PubMed: 17442842]

Malo C (1994). Free amino acid levels in serum and small intestine during the post-natal development of normal and sparse-fur mutant mice. Comp Biochem Physiol A Physiol 109, 1049–1057. [PubMed: 7828023]

Mancias JD, Wang X, Gygi SP, Harper JW, and Kimmelman AC (2014). Quantitative proteomics identifies NCOA4 as the cargo receptor mediating ferritinophagy. Nature 509, 105–109. [PubMed: 24695223]

Martin CR, Osadchiy V, Kalani A, and Mayer EA (2018). The Brain-Gut-Microbiome Axis. Cell Mol Gastroenterol Hepatol 6, 133–148. [PubMed: 30023410]

Matsumoto M, Kibe R, Ooga T, Aiba Y, Kurihara S, Sawaki E, Koga Y, and Benno Y (2012). Impact of intestinal microbiota on intestinal luminal metabolome. Sci Rep 2, 233. [PubMed: 22724057]

Matsumoto M, Ooga T, Kibe R, Aiba Y, Koga Y, and Benno Y (2017). Colonic Absorption of Low-Molecular-Weight Metabolites Influenced by the Intestinal Microbiome: A Pilot Study. PLoS One 12, e0169207. [PubMed: 28121990]

Parsons DS, and Shaw MI (1983). Use of high performance liquid chromatography to study absorption and metabolism of purines by rat jejunum in vitro. Q J Exp Physiol 68, 53–67. [PubMed: 6828647]

Pickard JM, Zeng MY, Caruso R, and Nunez G (2017). Gut microbiota: Role in pathogen colonization, immune responses, and inflammatory disease. Immunol Rev 279, 70–89. [PubMed: 28856738]

Ramakrishnan SK, Anderson ER, Martin A, Centofanti B, and Shah YM (2015). Maternal intestinal HIF-2alpha is necessary for sensing iron demands of lactation in mice. Proc Natl Acad Sci U S A 112, E3738–3747. [PubMed: 26124130]

Ramakrishnan SK, Zhang H, Ma X, Jung I, Schwartz AJ, Triner D, Devenport SN, Das NK, Xue X, Zeng MY, et al. (2019). Intestinal non-canonical NFkappaB signaling shapes the local and systemic immune response. Nat Commun 10, 660. [PubMed: 30737385]

Salim EI, Wanibuchi H, Morimura K, Kim S, Yano Y, Yamamoto S, and Fukushima S (2000). Inhibitory effects of 1,3-diaminopropane, an ornithine decarboxylase inhibitor, on rat two-stage urinary bladder carcinogenesis initiated by N-butyl-N-(4-hydroxybutyl)nitrosamine. Carcinogenesis 21, 195–203. [PubMed: 10657958]

Sanchez M, Galy B, Muckenthaler MU, and Hentze MW (2007). Iron-regulatory proteins limit hypoxia-inducible factor-2alpha expression in iron deficiency. Nat Struct Mol Biol 14, 420–426. [PubMed: 17417656]

Schaefer L, Auchtung TA, Hermans KE, Whitehead D, Borhan B, and Britton RA (2010). The antimicrobial compound reuterin (3-hydroxypropionaldehyde) induces oxidative stress via interaction with thiol groups. Microbiology 156, 1589–1599. [PubMed: 20150236]

Schott K, Huether G, and Neuhoff V (1983). Free amino acid concentrations in the gut lumen of developing rats. Biochem Med 29, 285–292. [PubMed: 6615488]

Schwartz AJ, Das NK, Ramakrishnan SK, Jain C, Jurkovic MT, Wu J, Nemeth E, Lakhal-Littleton S, Colacino JA, and Shah YM (2019). Hepatic hepcidin/intestinal HIF-2alpha axis maintains iron absorption during iron deficiency and overload. J Clin Invest 129, 336–348. [PubMed: 30352047]

Shah YM, Matsubara T, Ito S, Yim SH, and Gonzalez FJ (2009). Intestinal hypoxia-inducible transcription factors are essential for iron absorption following iron deficiency. Cell Metab 9, 152–164. [PubMed: 19147412]

Shankar V, Gouda M, Moncivaiz J, Gordon A, Reo NV, Hussein L, and Paliy O (2017). Differences in Gut Metabolites and Microbial Composition and Functions between Egyptian and U.S. Children Are Consistent with Their Diets. mSystems 2.

Siegert I, Schodel J, Nairz M, Schatz V, Dettmer K, Dick C, Kalucka J, Franke K, Ehrenschwender M, Schley G, et al. (2015). Ferritin-Mediated Iron Sequestration Stabilizes Hypoxia-Inducible Factor-1alpha upon LPS Activation in the Presence of Ample Oxygen. Cell Rep 13, 2048–2055. [PubMed: 26628374]

Smith PM, Howitt MR, Panikov N, Michaud M, Gallini CA, Bohlooly YM, Glickman JN, and Garrett WS (2013). The microbial metabolites, short-chain fatty acids, regulate colonic Treg cell homeostasis. Science 341, 569–573. [PubMed: 23828891]

Sridharan GV, Choi K, Klemashevich C, Wu C, Prabakaran D, Pan LB, Steinmeyer S, Mueller C, Yousofshahi M, Alaniz RC, et al. (2014). Prediction and quantification of bioactive microbiota metabolites in the mouse gut. Nat Commun 5, 5492. [PubMed: 25411059]

Talarico TL, and Dobrogosz WJ (1989). Chemical characterization of an antimicrobial substance produced by Lactobacillus reuteri. Antimicrob Agents Chemother 33, 674–679. [PubMed: 2751282]

Taylor M, Qu A, Anderson ER, Matsubara T, Martin A, Gonzalez FJ, and Shah YM (2011). Hypoxia-inducible factor-2alpha mediates the adaptive increase of intestinal ferroportin during iron deficiency in mice. Gastroenterology 140, 2044–2055. [PubMed: 21419768]

Vanoaica L, Darshan D, Richman L, Schumann K, and Kuhn LC (2010). Intestinal ferritin H is required for an accurate control of iron absorption. Cell Metab 12, 273–282. [PubMed: 20816093]

Wallace EM, Rizzi JP, Han G, Wehn PM, Cao Z, Du X, Cheng T, Czerwinski RM, Dixon DD, Goggin BS, et al. (2016). A Small-Molecule Antagonist of Hif2alpha Is Efficacious in Preclinical Models of Renal Cell Carcinoma. Cancer Res 76, 5491–5500. [PubMed: 27635045]

Wang Z, Klipfell E, Bennett BJ, Koeth R, Levison BS, Dugar B, Feldstein AE, Britt EB, Fu X, Chung YM, et al. (2011). Gut flora metabolism of phosphatidylcholine promotes cardiovascular disease. Nature 472, 57–63. [PubMed: 21475195]

Wikoff WR, Anfora AT, Liu J, Schultz PG, Lesley SA, Peters EC, and Siuzdak G (2009). Metabolomics analysis reveals large effects of gut microflora on mammalian blood metabolites. Proc Natl Acad Sci U S A 106, 3698–3703. [PubMed: 19234110]

Xue X, Taylor M, Anderson E, Hao C, Qu A, Greenson JK, Zimmermann EM, Gonzalez FJ, and Shah YM (2012). Hypoxia-inducible factor-2alpha activation promotes colorectal cancer progression by dysregulating iron homeostasis. Cancer Res 72, 2285–2293. [PubMed: 22419665]

Context and Significance

Iron is an element essential for almost all living organisms. Interestingly, both iron deficiency and excess are harmful and lead to globally important diseases such an anemia and iron overload. The intestine hosts a diverse indigenous microbial population known as gut microbiota, which relies on the iron coming from the host's diet for its survival. Researchers at the University of Michigan here show that Lactobacillus bacteria can sense intestinal iron levels and attenuate intestinal iron absorption by the host. Using relevant mouse models, the authors further show that mammalian iron disorders like iron deficiency anemia and iron overload can be therapeutically targeted by administering microbial species or regulating their metabolites.

Highlights

- Lactobacillus species sense intestinal iron levels and attenuate host iron absorption
- Microbial metabolites DAP and reuterin, are novel HIF-2α inhibitors
- Gut microbial metabolites regulate intestinal iron storage via ferritin regulation
- Gut microbiota can be therapeutically targeted for iron-related disorders

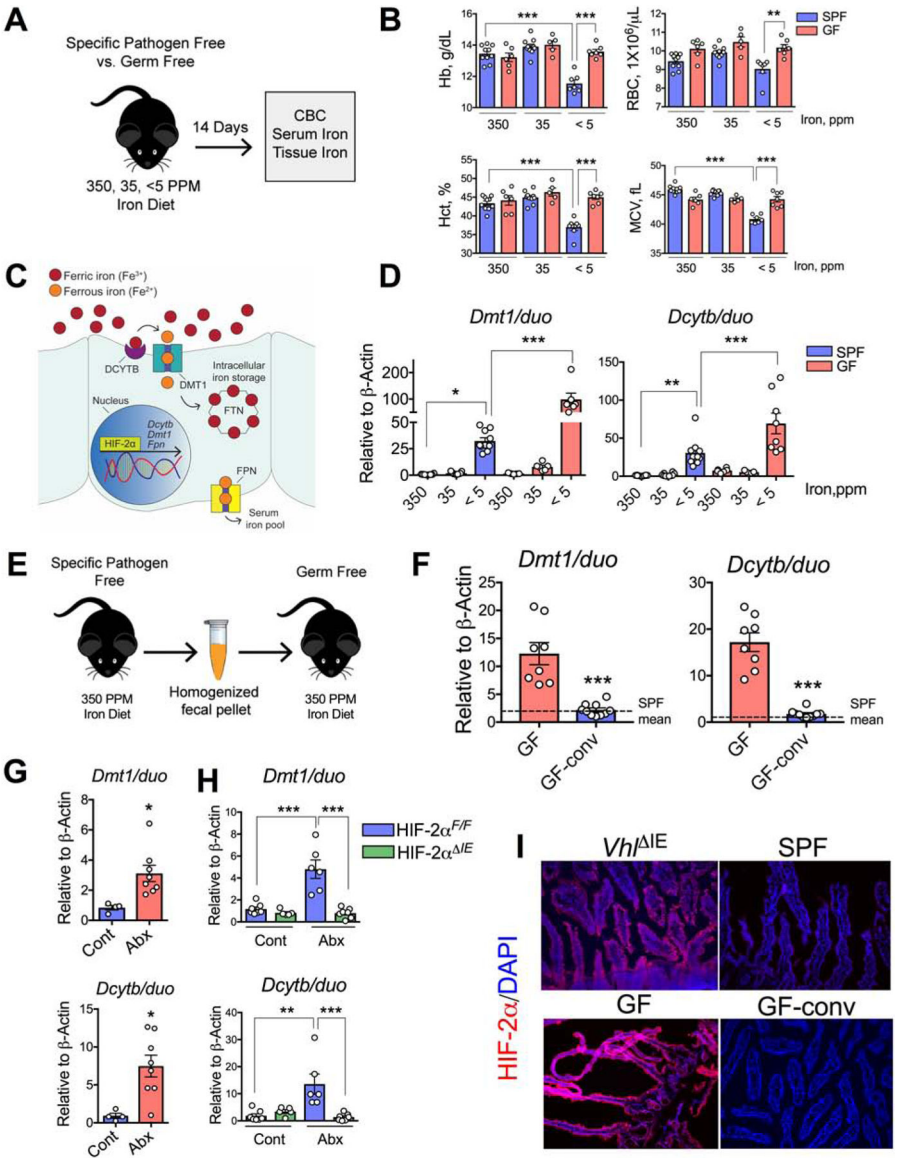

Figure 1. Gut microbiota suppress iron absorptive genes and HIF-2α expression.

A) Schematic of iron-diet treatment (350-, 35- and <5-ppm iron) in specific pathogen free (SPF) and germ free (GF) C57BL/6J mice, **B)** complete blood count (CBC). **C)** A general schematic of host intestinal iron regulation**. D)** Duodenal *Dmt1* and *Dcytb* gene expression in SPF and GF mice on 350-, 35- and <5 ppm iron diets. **E)** Schematic of conventionalization of GF gut (GF-conv) by SPF fecal suspension, and **F)** Duodenal *Dmt1* and *Dcytb* gene expression analysis of GF and GF-conv mice. Dotted lines indicate the corresponding mean gene expression values from SPF mice. **G)** SPF mice fed with standard chow diet (270-ppm iron) were depleted of microbiota by broad-spectrum antibiotic cocktail in the drinking water (Abx) and duodenal *Dmt1* and *Dcytb* gene expression analysis. **H)** Wild type (*Hif2*α$^{F/F}$) and intestine-specific HIF-2α knockout (*Hif2*α$^{\Delta IE}$) mice were treated with Abx, and duodenal *Dmt1* and *Dcytb* gene expression analyses shown. **I)**

Immunohistochemical analysis of HIF-2α in SPF, GF and GF-conv duodenum. Intestine-specific VHL knockout ($Vhl^{\Delta IE}$) used as positive control.

All data are mean ± SEM. One-way ANOVA with Tukey's multiple comparisons test (B, D and H) or t-test (F and G). * $P < 0.05$, ** $P < 0.01$, *** $P < 0.001$.

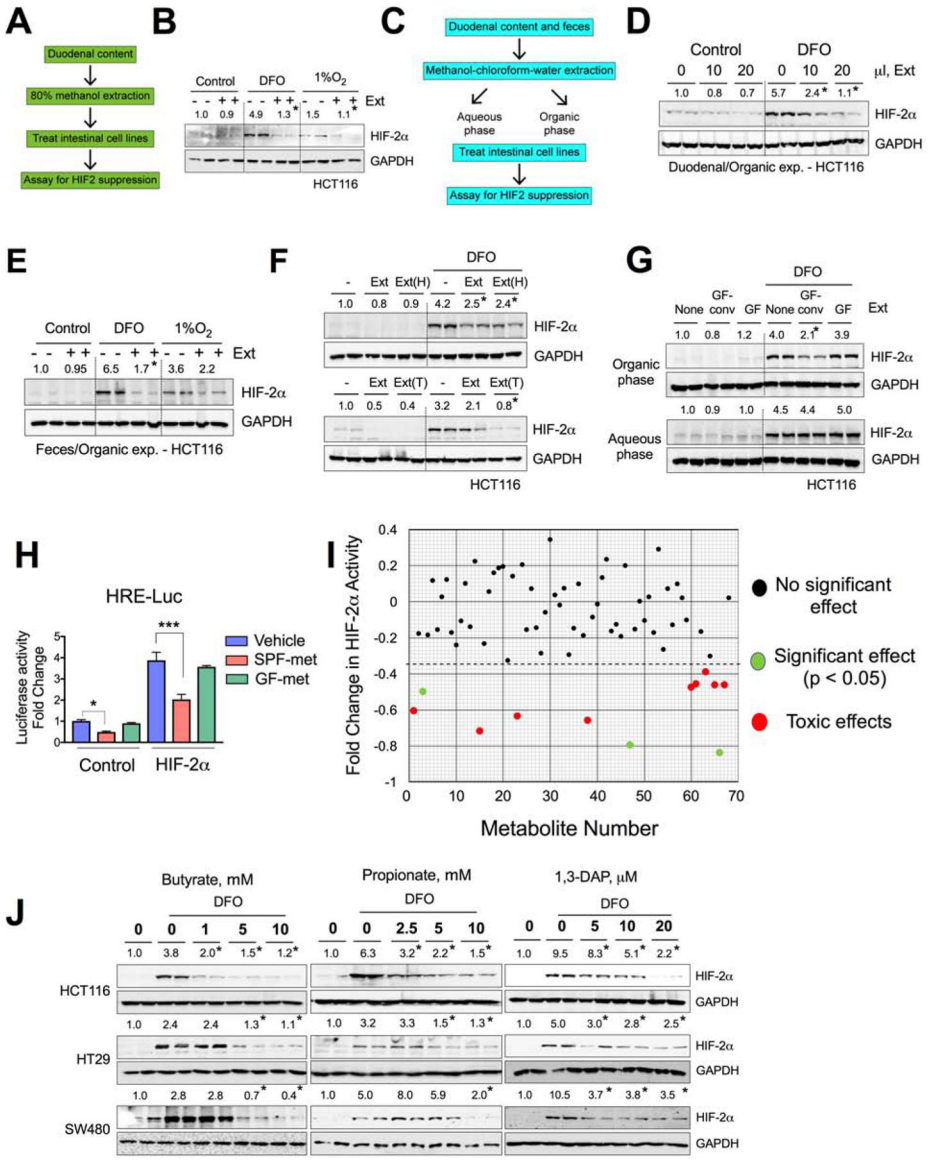

Figure 2. Microbial metabolites decrease HIF-2α expression and activity.

A) Schematic of duodenal metabolite extraction from wild type SPF mice and HIF-2α expression assay in intestinal cell lines, and **B)** HIF-2α Western analysis of DFO or 1% O_2 pretreated (4 hours) HCT116 cells followed by treatment with duodenal extracts (Ext) for 16 hours. **C)** Schematic of aqueous and organic extraction of duodenal and fecal metabolites from wild type SPF mice and HIF-2α expression assay in intestinal cell lines. HIF-2α Western analysis **(D and E)** in DFO- or 1% O_2 treated HCT116 cells or co-treated with organic extracts (Ext) for 16 hours. **(F)** HIF-2α Western analysis in DFO-treated HCT116 cells co-treated with Ext, heated (95°C) Ext [Ext(H)] (upper panel) or trypsin-digested Ext [Ext(T)] (lower panel) from fecal organic extracts. **G)** HIF-2α Western analysis in DFO-treated HCT116 cells or co-treated with organic (upper panel) and aqueous (lower panel) extracts from GF and GF-conv feces. **H)** HIF response element (HRE) luciferase assay (HRE-Luc) in HCT116 cells transfected with empty vector (control) or HIF-2α, followed by

treatment with vehicle (DMSO) or fecal organic extracts from SPF- (SPF-met) and GF (GF-met) mice (n=3). **I)** Metabolite screen for HIF-2α suppression based on HRE luciferase assay in HCT116 cells. **J)** HIF-2α Western analysis in DFO-treated or co-treated with butyrate, propionate and 1,3 diaminopropane (DAP) in HCT116, HT29 and SW480 cells. All data are mean ± SEM. One-way ANOVA with Tukey's multiple comparisons test (H and I). Western analyses (B, D, E, F, G and J): Images were analyzed by Image J software from three independent experiments, representative image shown. Statistical significance compared with DFO-only or 1% O_2–only (B and E) treatment group. * $P < 0.05$, *** $P < 0.001$.

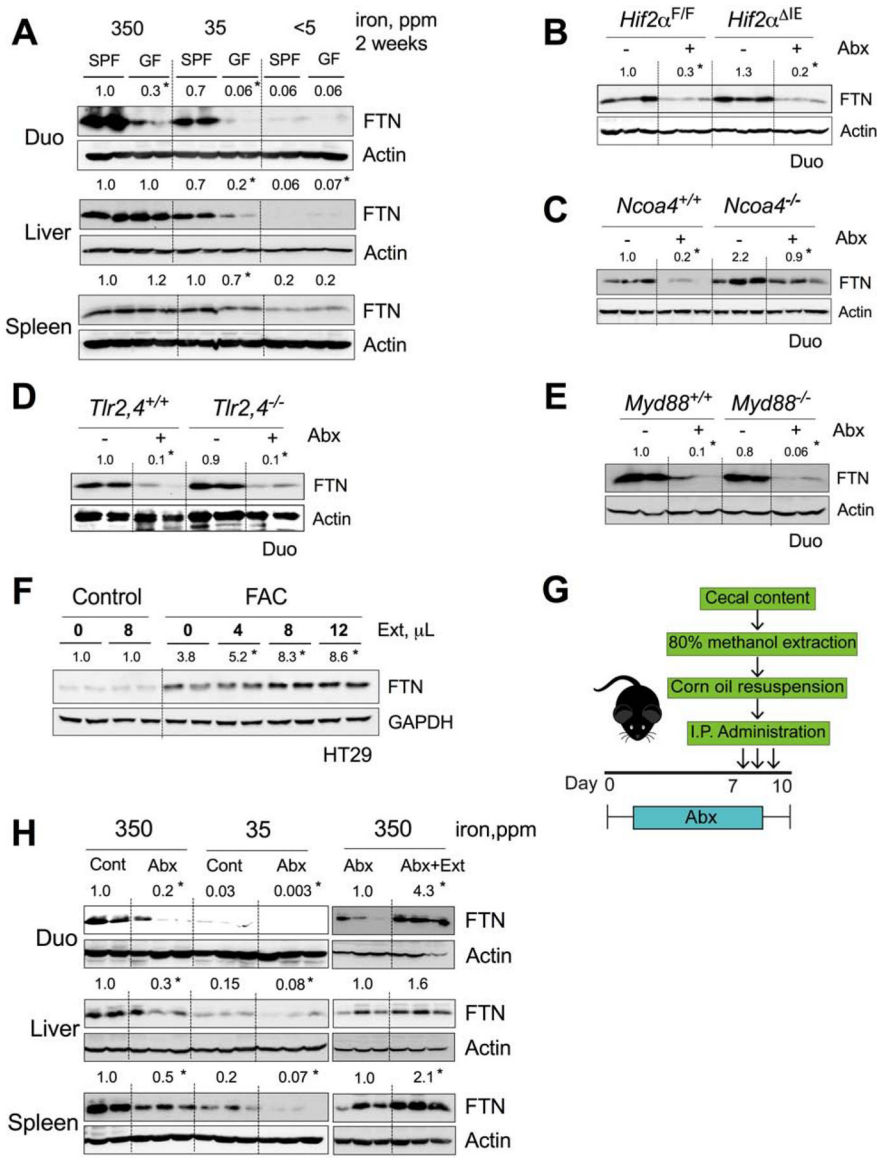

Figure 3. Microbial metabolites sustain intestinal and peripheral tissue ferritin (FTN) expression.

FTN Western analyses in **A)** duodenum, liver and spleen of SPF vs. GF mice fed with 350-, 35- or <5-ppm iron diet; and duodenum of control or Abx treated, **B)** wild type (*Hif2*α$^{F/F}$) and intestine-specific HIF-2α knockout (*Hif2*α$^{\Delta IE}$) mice, **C)** wild type (*Ncoa4*$^{+/+}$) and NCOA4 knockout (*Ncoa4*$^{-/-}$) mice, **D)** wild type (*Tlr2,4*$^{+/+}$) and TLR2,4 double knockout (*Tlr2,4*$^{-/-}$) mice, and **E)** wild type (*Myd88*$^{+/+}$) and Myd88 knockout (*Myd88*$^{-/-}$) mice. **F)** FTN Western analysis of ferric ammonium citrate (FAC, 10μM) pretreated HT29 cells followed by dose-dependent treatment of fecal metabolites from wild type SPF mice. **G)** Schematic showing Abx treatment of wild type C57BL/6J mice followed by intraperitoneal (i.p.) injection of fecal metabolites (Ext). **H)** FTN Western blot analyses of duodenum liver and spleen of control or Abx treated mice fed with 350- and 35 ppm iron diet (left panel), and Abx or Abx plus Ext treated mice fed with 350 ppm iron diet (right panel).

All data are mean ± SEM. Western analyses (A-F and H): Images were analyzed by Image J software from three independent experiments, representative image shown. Statistical significance compared within the respective groups (A-E and H) and FAC-only control (F). * $P < 0.05$

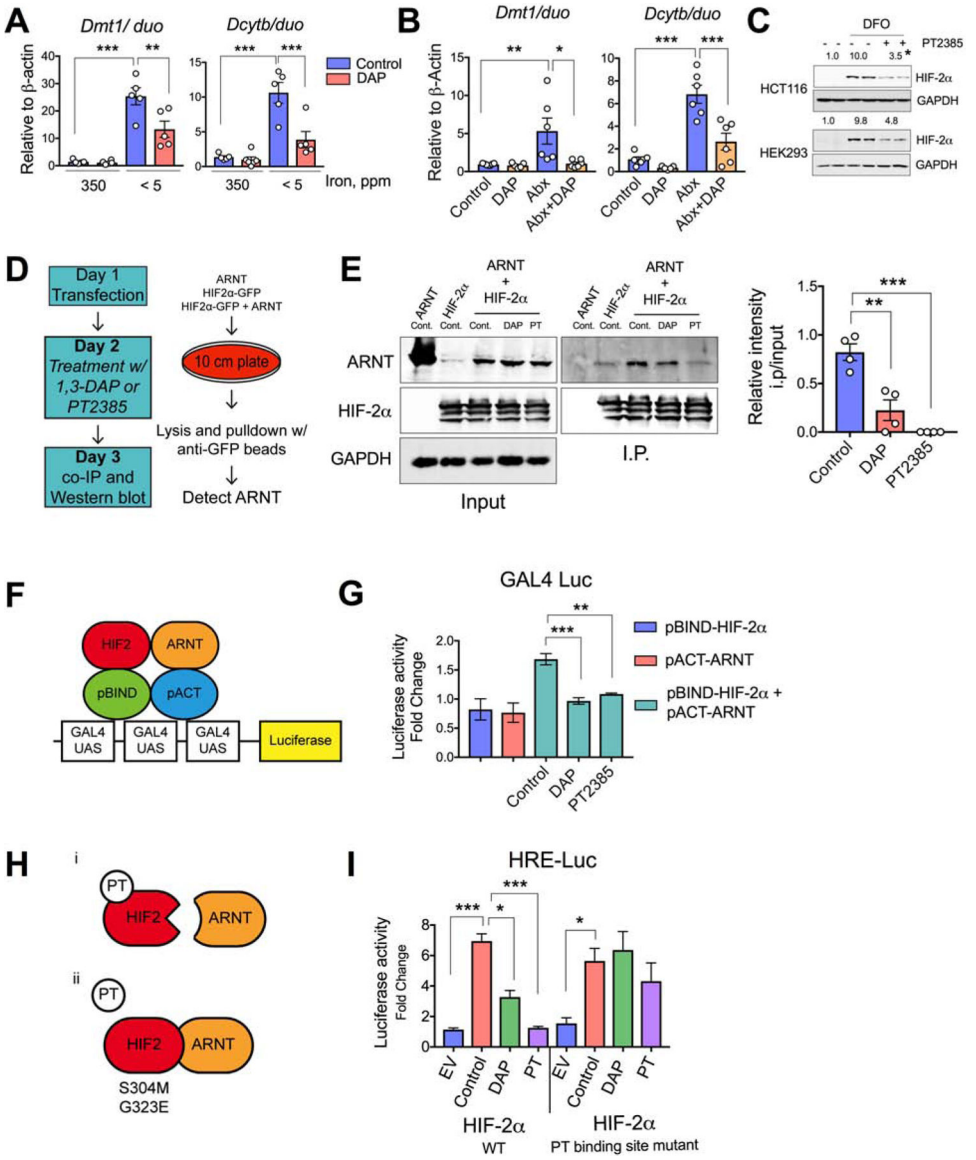

Figure 4. DAP suppresses HIF-2α activity *in vivo* via blocking heterodimerization.

Duodenal *Dmt1* and *Dcytb* gene expression in C57BL/6 wild type SPF mice **A)** fed with 350- or < 5 ppm iron diet and treated with 1,3 diaminopropane (DAP) in drinking water (2g/L) for 2 weeks, or **B)** treated with antibiotic cocktail (Abx) and/or DAP in drinking water for 2 weeks. **C)** HIF-2α Western analysis of DFO-treated HCT116 and HEK293 cells followed by PT2385 treatment. **D)** Schematic of co-immunoprecipitation protocol for determination of the roles of DAP or PT2385 in HIF-2α-ARNT interaction. **E)** Co-immunoprecipitation for ARNT and HIF-2α in HEK-293T cells treated with DAP (50μM) or PT2385 (10μM); Relative densitometric analysis of four independent experiment shown on the right panel. **F)** Schematic and **G)** experimental representation of DAP- or PT-mediated HIF-2α-ARNT interaction by pG5GAL4 luciferase assay followed by pBIND-HIF-2α and/or pACT-ARNT transfection of HEK293 cells (n=3). **H)** Schematic showing effect of PT2385 or PT2399 (PT) on HIF-2α-ARNT interaction and the effect on the same

following the mutation of PT2385 or PT2399 binding sites on HIF-2α. **I)** HEK293 cells were transfected with wild type or PT-binding site mutant HIF-2α followed by DAP or PT treatment, and HRE luciferase assay performed (n=3).

All data are mean ± SEM. One way ANOVA with Tukey's multiple comparisons test (A, B, E right panel, G and I). Western analyses (C): Images were analyzed by Image J software from three independent experiments, representative image shown. Statistical significance compared with DFO-only treatment group. * $P < 0.05$, ** $P < 0.01$, *** $P < 0.001$.

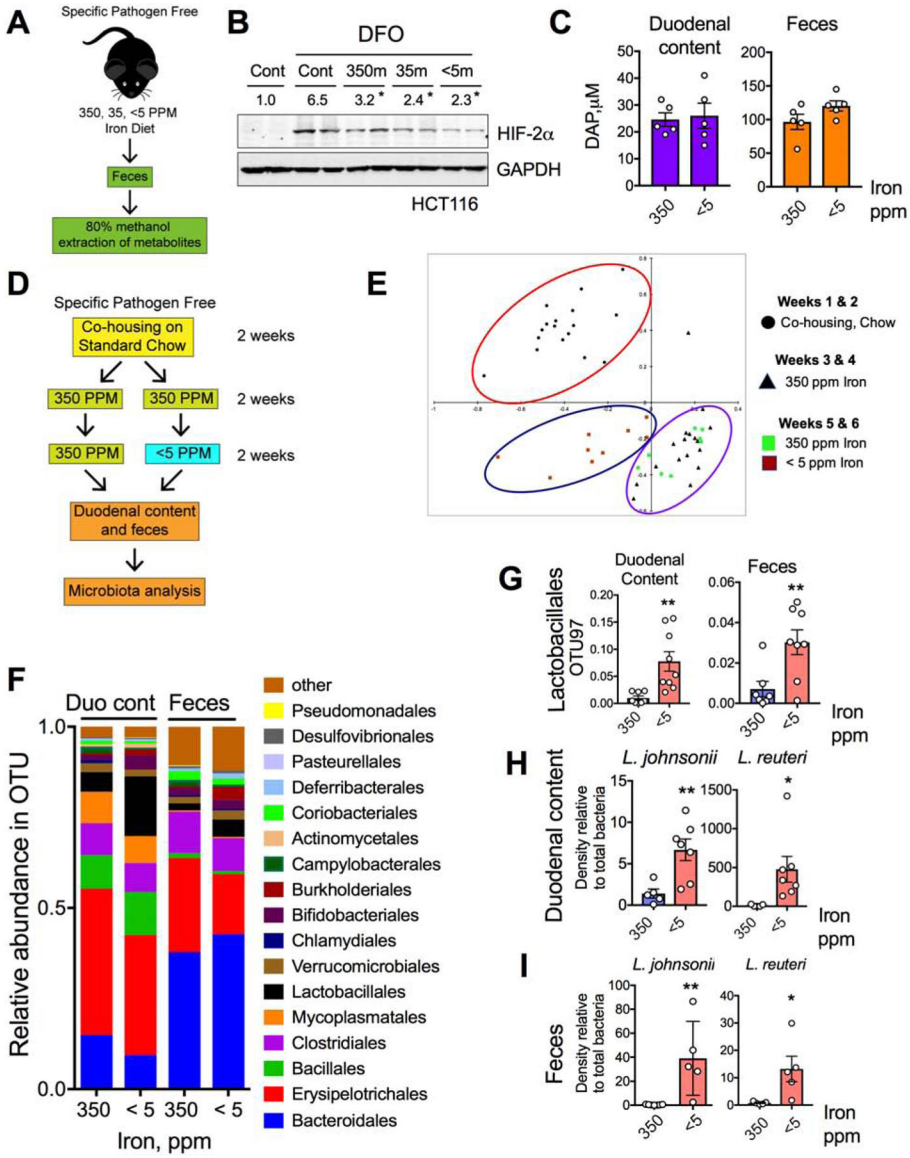

Figure 5. Low-iron diet potentiates HIF-2α inhibition by microbial metabolites.

A) Schematic of fecal metabolite extraction from SPF mice fed with 350-, 35- and < 5-ppm iron diet for 2 weeks and **B)** HIF-2α Western analysis in HCT116 cells treated with or without DFO and metabolites (350m, 35m or <5m respectively). **C)** DAP concentration in duodenum and feces from wild type fed with 350- and <5-ppm iron diet for two weeks. **D)** Schematic of the experimental set up for bacterial community analysis. **E)** Principal component analysis (PCA) of fecal bacterial population from 16S rRNA sequencing data in mice fed with 350-ppm and < 5-ppm iron diet. **F)** 16S rRNA sequencing bacterial community analysis from duodenal content and feces. **G)** Comparative analysis of genus *Lactobacillales* by OTU97 (97% sequence similarity) values in duodenal content and feces. Comparative analysis of *L. johnsonii* and *L. reuteri* density by species specific PCR from **H)** duodenal content and **I)** feces.

All data are mean ± SEM. t-test for the corresponding panels (C, G, H, I). Western analyses (B): Images were analyzed by Image J software from three independent experiments, representative image shown. Statistical significance compared with DFO-only treatment group. * $P < 0.05$, ** $P < 0.01$.

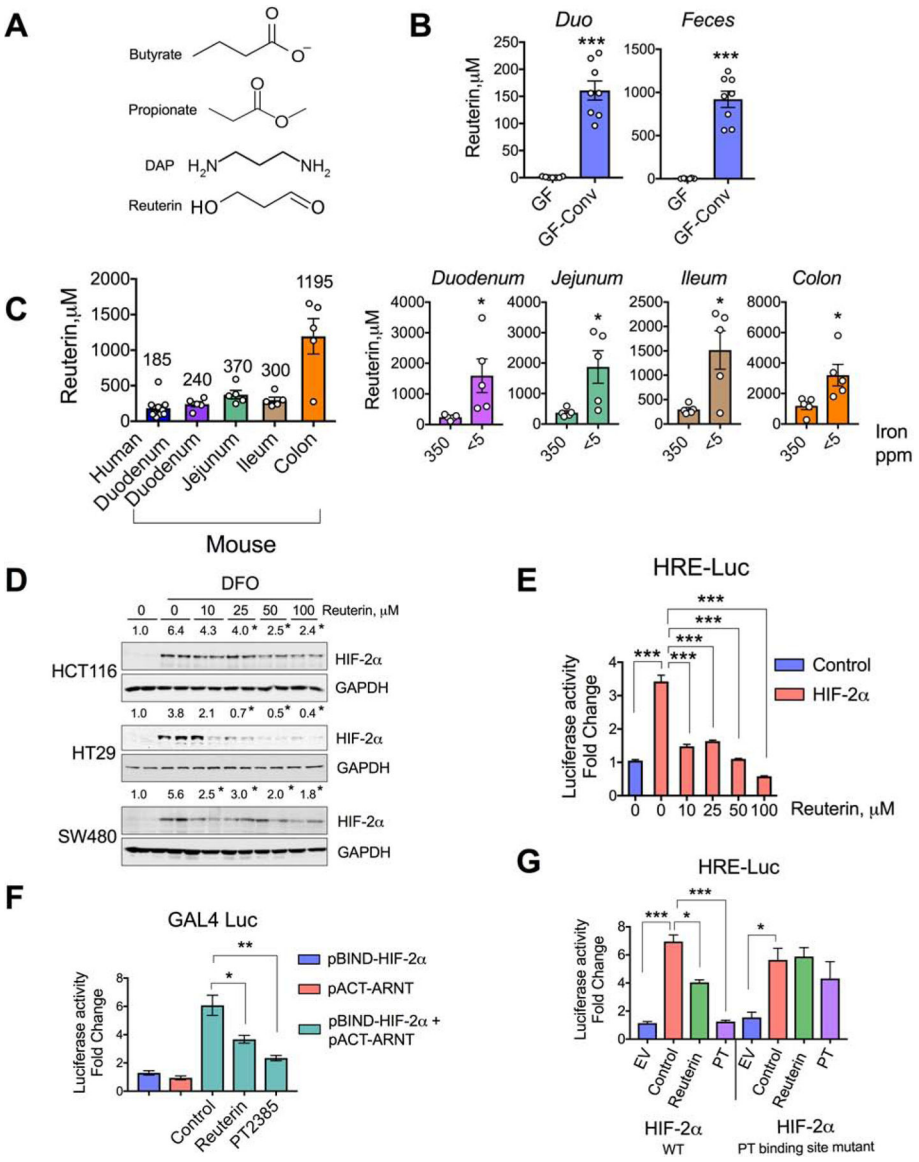

Figure 6. Reuterin suppresses HIF-2α activity via blocking heterodimerization.

A) Chemical structures of butyrate, propionate, DAP and reuterin. **B)** Intestinal reuterin concentrations in GF and GF-conv mice. **C)** Mean physiological concentration of reuterin in the human duodenum and mouse intestine (left panel) and intestinal reuterin concentration in mice fed with 350-ppm or < 5-ppm iron diet (right panel). **D)** HIF-2α Western analysis in DFO treated HCT116, HT29 and SW480 cells or co-treated with reuterin. **E)** HRE luciferase assay in HCT116 cells transfected with empty vector (control) or HIF-2α, followed by dose-dependent treatment of reuterin (n=3). **F)** Modified two-hybrid assays in HEK293 cells transfected with pBIND-HIF-2α and pACT-ARNT and treated with reuterin or PT2385 (PT) (n=3). **G)** HRE-luciferase assay in HEK293 cells transfected with wild type or PT-binding site mutant of HIF-2α and treated with reuterin or PT2385 (PT) (n=3).

All data are mean ± SEM. t-test (B and C) or one-way ANOVA with Tukey's multiple comparisons test (E, F and G). Western analyses (D): Images were analyzed by Image J

software from three independent experiments, representative image shown. Statistical significance compared with DFO-only treatment group. * $P < 0.05$, ** $P < 0.01$, *** $P < 0.001$.

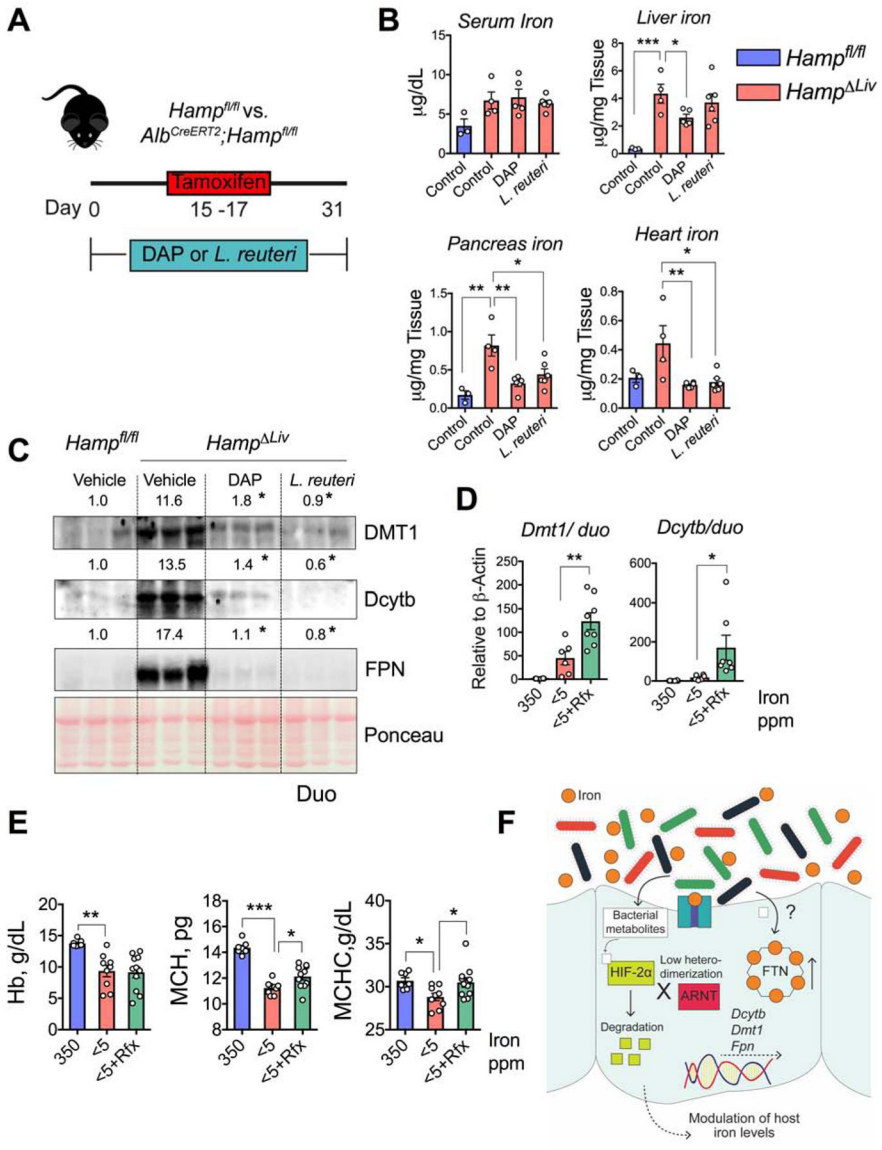

Figure 7. DAP and reuterin prevent systemic iron accumulation and antibiotics improve anemia in mouse models.

A) Schematic showing timeline of DAP or *L. reuteri* probiotic treatment in tamoxifen-mediated temporal disruption of hepcidin (*Hamp*$^{\Delta Liv}$). **B)** Serum and tissue (liver, pancreas and heart) iron analyses and **C)** Duodenal DMT1, Dcytb and FPN Western analyses in DAP- or *L. reuteri* probiotic treated *Hamp*$^{fl/fl}$ and *Hamp*$^{\Delta Liv}$ mice. Wild type SPF mice were fed with 350- or <5-ppm iron diet for 1 week followed by 350-ppm, <5-ppm or rifaximin (Rfx) (20 mg/kg/day)-blended <5-ppm diet for another 2 weeks; **(D)** duodenal *Dmt1* and *Dcytb* gene expression and **(E)** CBC (Hb, MCH and MCHC) analysis. **F)** Schematic showing integration of HIF-2α inhibitory and FTN stimulatory roles of gut microbial metabolites to regulate host systemic iron homeostasis. HIF-2α inhibitory metabolites disrupt HIF-2α-ARNT interaction followed by its degradation and subsequent transcriptional downregulation of the intestinal transporters, a different subset of metabolites upregulates FTN expression. Both of these responses can lead to decreased iron absorption.

All data are mean ± SEM. One-way ANOVA with Tukey's multiple comparisons test (B, D and E). Western analyses (C): Images were analyzed by Image J software from three independent experiments, representative image shown. Statistical significance compared with Vehicle-only treatment group. * $P < 0.05$, ** $P < 0.01$, *** $P < 0.001$.